Identification of New Orbits to Enable Future Mission Opportunities for the Human Exploration of the Martian Moon Phobos[☆]

Mattia Zamaro[1,*], James D. Biggs[2,*]

Advanced Space Concepts Laboratory, University of Strathclyde, 75 Montrose Street, G1 1XJ, Glasgow, United Kingdom

Abstract

One of the paramount stepping stones towards NASA's long-term goal of undertaking human missions to Mars is the exploration of the Martian moons. Since a precursor mission to Phobos would be easier than landing on Mars itself, NASA is targeting this moon for future exploration, and ESA has also announced Phootprint as a candidate Phobos sample-and-return mission. Orbital dynamics around small planetary satellites are particularly complex because many strong perturbations are involved, and the classical circular restricted three-body problem (R3BP) does not provide an accurate approximation to describe the system's dynamics. Phobos is a special case, since the combination of a small mass-ratio and length-scale means that the sphere-of-influence of the moon moves very close to its surface. Thus, an accurate nonlinear model of a spacecraft's motion in the vicinity of this moon must consider the additional perturbations due to the orbital eccentricity and the complete gravity field of Phobos, which is far from a spherical-shaped body, and it is incorporated into an elliptic R3BP using the gravity harmonics series-expansion (ER3BP-GH). In this paper, a showcase of various classes of non-keplerian orbits are identified and a number of potential mission applications in the Mars-Phobos system are proposed: these results could be exploited in upcoming unmanned missions targeting the exploration of this Martian moon. These applications include: low-thrust hovering and orbits around Phobos for close-range observations; the dynamical substitutes of periodic and quasi-periodic Libration Point Orbits in the ER3BP-GH to enable unique low-cost operations for space missions in the proximity of Phobos; their manifold structure for high-performance landing/take-off maneuvers to and from Phobos' surface and for transfers from and to Martian orbits; Quasi-Satellite Orbits for long-period station-keeping and maintenance. In particular, these orbits could exploit Phobos' occulting bulk and shadowing wake as a passive radiation shield during future manned flights to Mars to reduce human exposure to radiation, and the latter orbits can be used as an orbital garage, requiring no orbital maintenance, where a spacecraft could make planned pit-stops during a round-trip mission to Mars.

Keywords: Phobos, Mars manned mission, Libration Point orbits, Quasi-Satellite orbits, Artificial Equilibrium points, radiation shielding
2010 MSC: 70F15, 70G60, 70Kxx, 37D05
PACS: 91.10.Sp, 95.55.Pe, 96.30.Hf, 95.10.Ce, 45.50.Pk, 98.70.Sa

List of Acronyms

2B	Two-Body
2B-P	Perturbed Two-Body
3B	Three-Body
2BP	Two-Body Problem
3BP	Three-Body Problem

[☆]This paper was presented during the 65th International Astronautical Congress, Toronto, Canada.

[*]Corresponding author
Email addresses: mattia.zamaro@strath.ac.uk (Mattia Zamaro), james.biggs@strath.ac.uk (James D. Biggs)
[1]+44 (0) 141 574 5025
[2]+44 (0) 141 574 5011

AEP	Artificial Equilibrium Point
BCBF	Body-Centered Body-Fixed
CR3BP	Circular Restricted Three-Body Problem
CR3BP-CA	Circular Restricted Three-Body Problem with Constant Acceleration
CR3BP-GH	Circular Restricted Three-Body Problem with Gravity Harmonics
ER3BP	Elliptic Restricted Three-Body Problem
ER3BP-GH	Elliptic Restricted Three-Body Problem with Gravity Harmonics
Ef.D.	Effective Dose
GCR	Galactic Cosmic Ray
GH	Gravity Harmonic
GNC	Guidance, Navigation and Control
IM	Invariant Manifold
LP	Libration Point
LPO	Libration Point Orbit
MRP	Mars Radiation Pressure
OE	Orbital Element
PO	Periodic Orbit
PRP	Phobos Radiation Pressure
QPO	Quasi-Periodic Orbit
QSO	Quasi-Satellite Orbit
R3BP	Restricted Three-Body Problem
R4BP	Restricted Four-Body Problem
SEP	Solar Electric Propulsion
SEPE	Solar Energetic Particle Event
SOI	Sphere of Influence
SRP	Solar Radiation Pressure
SS	Sun-Synchronous
VDCO	Vertical-Displaced Circular Orbit

1. Introduction

Since the discovery of Phobos and Deimos in 1877, the two natural satellites of Mars have become increasingly interesting astronomical objects to investigate. Phobos is closer to Mars than Deimos and almost double its size, but despite this, they are very similar, since they share common physical, orbital and geometrical features. Their origin is still largely unknown [1, 2], and is currently debated to have been either an asteroid capture by Mars, or coalescence from proto-Mars or Solar System material, or even accretion of material from Mars ejected from its surface after an impact with a previous small body. This puzzle is supported by the mysterious composition of these moons inferred from infrared spectral analysis: due to their relative low density and high porosity, they could hide a considerable amount of iced water [2], which is an attractive in-situ resource that could be exploited by human missions. In addition, it is speculated that the Martian moons' rocks could provide evidence of alien life [3]. Phobos has some unique characteristics that make it also astrodynamically interesting. The low altitude of its orbit around Mars has produced speculation on its evolution: due to its tidal interaction with Mars, its altitude is currently decreasing, which means Phobos will eventually crash into Mars or break up into a planetary ring [4].

Due to its proximity to Mars, Phobos is currently of great interest for future missions to the Red Planet. During its Ministerial Council Meeting of November 2012, ESA confirmed post-2018 mission concepts: the Mars Robotic Exploration Programme would include a mission (Phootprint) to return back to Earth a sample from Phobos [5, 6]. Another sample-and-return mission to this moon is currently proposed by NASA Innovative Advanced Concepts team, that will use two CubeSats propelled by a solar sail and joined by a tether mechanism [7]. In addition, NASA has identified a mission to Phobos as a key milestone to be achieved before bringing humans to Mars [8, 9, 10, 11], since the absence of atmosphere on Phobos and Deimos makes landing and take-off easier for a manned spacecraft than on Mars. Therefore, the Martian moons could be exploited as outposts for astronauts: Phobos' proximity and fast orbital period can provide a relay for robotic exploration on Mars, and protection from space radiation hazards for manned spacecraft orbiting Mars (Phobos' bulk and shadow shielding the spacecraft). At the beginning of 2013, with the development of a new rover platform for the exploration of minor bodies, consisting of robotic hedgehogs, it has been reported that NASA is taking into consideration a mission (Surveyor) to Phobos as a test-bed for this new technology [12].

The purpose of this paper is to present a breakdown of different kinds of orbits that could be exploited in future space missions to Phobos. In [13], a collection of different options that a spacecraft can use to orbit around Phobos is discussed, and their properties are preliminarily assessed in the framework of the three-body dynamics. This paper builds on this approach by expanding the compu-

tation to all the available orbits within each class of trajectories, refined in more tailored models of the relative dynamics, and by computing a broad range of their properties for space engineering applications. These results will become useful for the ultimate selection of the operative orbits in the mission design loop to plan the exploration of Phobos.

The outline of this paper is as follows. Section 2 introduces the reader to the physical environment connected to the orbital dynamics and constraints of a spacecraft in the vicinity of Phobos. The following sections 3-6 showcase each of the different kinds of orbits around this moon, such as: hovering points using Solar Electric Propulsion (SEP); Vertical Displaced Circular Orbits with low-thrust; natural Libration Point Orbits and their Invariant Manifold trajectories, and their artificial equivalent with constant low-thrust; Quasi-Satellite Orbits around Phobos. Section 7 provides a summary of the different solutions focusing on their applications in space missions to Phobos. Section 8 concludes the paper suggesting their potential usefulness in a real-world mission scenario.

2. Preliminary Analysis for a Space Mission around Phobos

In this section we introduce the basic design aspects of the dynamics and physics of a spacecraft in orbit of Phobos.

2.1. Physical and Astrodynamical Characteristics

The immediately noticeable characteristics of Phobos are its small size (even smaller than some asteroids) and its irregular shape: in particular the surface is marked by a dense texture of grooves and by several big craters, one of them, named Stickney, is by far the largest and is located on the face of the moon pointing towards Mars. Phobos has an almost circular and equatorial orbit around Mars, and it rotates with synchronous period and almost zero-tilt with respect to its orbital motion. The low altitude of its orbit is lower than that required for a Mars-synchronous rotation: Phobos rises from the West more than three times a day as seen from Mars' surface near its Equator, whereas near the poles Phobos is never seen, since it is always under the horizon. Table 1 presents a summary of the physical and orbital parameters of Mars and Phobos that have been used in the analysis of the orbits undertaken in this paper.

Table 1: **Physical and astrodynamical properties.** The values are retrieved from the following sources. Ephemerides: NASA JPL at 25th July 2012 00.00CT (ICRF/J2000.0). Phobos axial tilt θ at date: mean value at epoch 1.08°. Gravity models: Mars MGM1025, Phobos [14].

Property	Mars	Phobos
$m\ [kg]$	$6.42 \cdot 10^{23}$	$1.07 \cdot 10^{16}$
Size $[km]$	R mean sphere $3.39 \cdot 10^3$	R mean ellipsoid $13.1 \times 11.1 \times 9.3$
Revolution T	$687d$	$7.65h$
Rotation T	$24.6h$	$7.65h$
θ [°]	25.19	0.30
Gravity Field	GHs	GHs
J_2	0.00196	0.105
$J_{2,2}$	0.0000631	0.0147
J_3	0.0000315	0.00775
J_4	0.0000154	0.0229
Orbital Elements	Sun-Ecliptic	Mars-Equatorial
$a\ [km]$	$2.28 \cdot 10^8$	$9.38 \cdot 10^3$
e	0.0934	0.0156
i [°]	1.85	1.07

2.2. Relative Dynamics

The general equations of motion of the relative orbital dynamics that will be used to describe the different kinds of orbits presented in this paper are stated in Eq.1,

$$\ddot{\mathbf{q}} = -\mathbf{a_A} + \mathbf{a_G} + \mathbf{a_P} + \mathbf{a_C} + \mathbf{a_D} \tag{1}$$

$$\mathbf{a_A} = \mathbf{a_{A,T}} + \boldsymbol{\omega} \wedge \boldsymbol{\omega} \wedge \mathbf{q} + \dot{\boldsymbol{\omega}} \wedge \mathbf{q} + 2\boldsymbol{\omega} \wedge \dot{\mathbf{q}} \tag{2}$$

where $\mathbf{q}$ is the position of the spacecraft and $\mathbf{a_A}$ is the apparent acceleration of the general relative frame of reference. $\mathbf{a_A}$ is presented in Eq.2 as a function of the frame's translational acceleration $\mathbf{a_{A,T}}$ and angular velocity $\boldsymbol{\omega}$ with respect to an inertial reference; $\mathbf{a_G}$ is the sum of the gravity accelerations of the celestial bodies of interest, each defined as the gradient of the gravitational potential $u_{G,\oplus} = Gm_\oplus/||\mathbf{q} - \mathbf{q}_\oplus||$, where G is the gravitational constant, $m_\oplus$ and $\mathbf{q}_\oplus$ are the mass and position of the body $\oplus$; $\mathbf{a_P}$ indicates the thrusting acceleration of the propulsion system of the spacecraft required for artificial orbits, while for natural orbits $\mathbf{a_P} = \mathbf{0}$. These three terms constitute the model of the dynamics where the reference signal of the orbit over time $\mathbf{q}(t)$ is solved, to be used by the guidance system in the mission. This motion will be perturbed in the real world by the disturbance $\mathbf{a_D}$, consisting of the forces not considered in the model, and by the perturbations on the initial condition $\mathbf{q_0}$, due to the inaccuracies of the navigation system; to track the guidance law, such per-

turbations need to be counteracted by the station-keeping action $\mathbf{a_C}$ of the orbital control system of the spacecraft, either planned in feedforward or performed in feedback.

The study of the dynamics of a spacecraft about Phobos is conducted in the first instance with the model of the classical circular restricted three-body problem (CR3BP) [15], where the two massive bodies are Mars (1) and Phobos (2), and the frame of reference is centered in the Mars-Phobos barycenter and aligned with the rotating Hill's frame of the Mars-Phobos orbit, which is considered keplerian, circular, and equatorial. The equations of motion of the CR3BP are derived from Eq.1 using a constant vertical $\boldsymbol{\omega}$ corresponding to the Mars-Phobos mean motion, and considering the gravity $\mathbf{a_{G_1}}$ and $\mathbf{a_{G_2}}$ of the two massive bodies placed in fixed position in this frame's choice. Using non-dimensional units, the only parameter of the CR3BP is the mass factor μ, the normalized mass of the secondary body with respect to the total mass of the primaries, while the semi-major axis of their orbit provides the length unit l[3]. For the case of Mars and Phobos, two peculiarities are evident from the physical parameters of Table 1: the mass parameter of the system is very small ($\mu = 1.66 \cdot 10^{-8}$), if compared to other cases studied so far in the Solar System, and the length unit of the system is very small too since the altitude of Phobos' orbit is less than twice the radius R_1 of Mars ($R_1/l = 36\%$), an unusual condition for a pair of primaries in our Solar System.

The Hill's sphere of influence (SOI) is the region around each body where the dynamics is dominated by its own gravity field, and its radius for Phobos is 0.17% of the distance from Mars, and considering the fact that Phobos is very irregular in shape the related maximum altitude is only $3.5km$, therefore it is impossible to naturally orbit around Phobos with a Keplerian motion, as shown in Fig.1. In particular the microgravity environment of Phobos is characterized by a keplerian escape velocity at its mean surface of only $11m/s$, which means a human being (or a rover) could auto-inject itself out of the body with a very small force.

The collapse of the realm of attraction of the secondary body of the CR3BP towards its surface is a result of the two peculiarities of the Mars-Phobos system, which has some additional physical and orbital features: not only the revolution of Pho-

[3] x,y,z axes in all the figures are normalized in l units unless otherwise indicated.

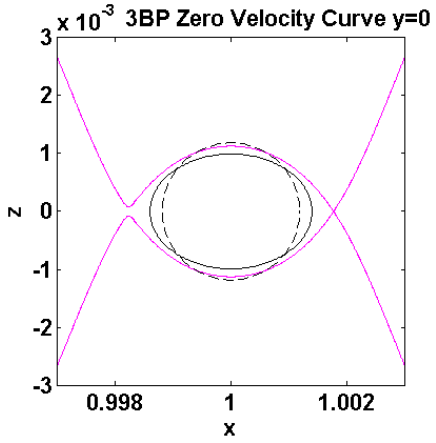

Figure 1: **Hill's surface for L_2 energy.** x-z projection. Phobos mean sphere (dashed line) and ellipsoid (plain line).

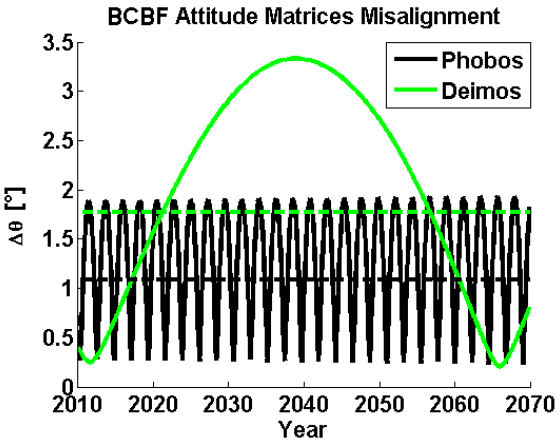

Figure 2: **Misalignment angle between the equatorial and orbital planes of the Martian moons.** Mean values dotted.

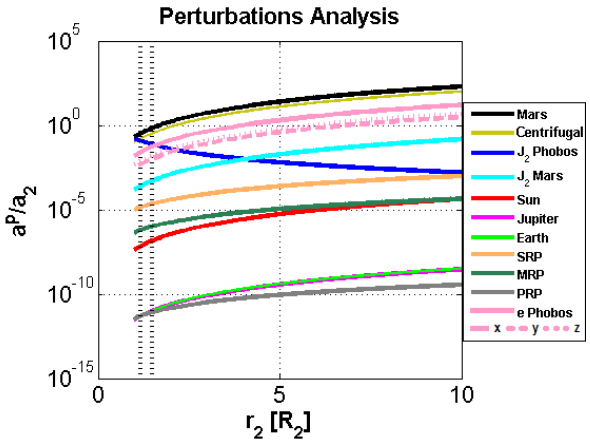

Figure 3: **Differential perturbations analysis.** Vertical dotted lines indicate Phobos major size and Hill's SOI radius.

bos around Mars and the rotation around its spin axis are synchronous, but they are also respectively equatorial and zero-tilted [16], therefore Phobos' attitude, expressed by the body-centered body-fixed reference frame BCBF, is approximately fixed in the rotating frame of the CR3BP, and so they differ only by the definition of the Prime Meridian [17, 16]. Before this choice, the actual misalignment between the two frames oscillates between a minimum of 0.30° and a maximum of 1.90°, and the dynamics of this libration motion is much slower than the time-scale of a mission segment around Phobos (period of 2.26 terrestrial years), as presented in Fig.2.

2.3. Orbital Perturbations

An analysis is undertaken to quantify approximately the errors that occur in the Mars-Phobos system when it is approximated with a CR3BP. The major physical orbital perturbations are distinguished by gravitational and non-gravitational forces. In the first class, we have the net term that when added to the basic newtonian point-mass force provides the true gravity pull of a general non-spherical and non-uniform body, which is usually modeled with a spherical harmonics series expansion known as gravity harmonics (GHs): for a first analysis, we consider the dominant term for both Mars and Phobos gravity fields, which is known as J_2 and is related to the oblateness of the body; the second type of gravitational perturbation is the basic gravitational term of additional bodies, that in the framework of the 3BP is referred as a fourth body perturbation, which is the sum of the body gravity and its apparent force on the 3BP frame: for a basic analysis, we consider the perturbing body in the closest conjunction configuration with Phobos. In the second class, we have the pressure disturbances of the atmospheric drag and the electromagnetic radiation: Phobos does not have an atmosphere, and the atmosphere of Mars is negligible at Phobos' altitude, therefore we consider the radiation pressures of the Sun (SRP), Mars (MRP, enclosing also the portion of the albedo of the SRP), and Phobos (PRP, with its albedo). These perturbations require knowledge of additional technical parameters of the structure and the subsystems of the spacecraft, so for a first analysis we consider common mean values for them. In addition to these physical actions, we must consider the modeling perturbations represented by the approximation of the dynamics as a circular R3BP, which is the effect of the eccentricity of the Mars-Phobos orbit. To derive a related physical acceleration value, we consider the difference between the acceleration field of the CR3BP and the one of the elliptic R3BP of the Mars-Phobos system, where $\boldsymbol{\omega}$ and the primaries' positions are variable, and we take the maximum over the orbital phases of Phobos, with the reference of the same relative state with respect to Phobos.

An important point to consider is that Phobos' orbit around Mars is not keplerian, but it seems to follow a classical low altitude J_2 perturbed orbit. Therefore, the analysis of every orbital perturbation which is not due to Phobos (gravity and PRP) in its proximity must be conducted in the framework of the relative dynamics with respect to Phobos, considering the resulting differential perturbation.

Since this analysis is undertaken to derive a basic reference for the orbital perturbations, it will be applied for the simple case of fixed relative points. Also, as we are interested in the dynamics near Phobos, due to the small size of its SOI, all the perturbations are nearly isotropic, and the only variable for this simple analysis is the radial distance from Phobos along the Mars-Phobos direction (apart from the eccentricity, which has been evaluated along all three directions). Outcomes of the differential analysis are presented in Fig.3, where the perturbations are shown as a ratio $\mathbf{a^P}/\mathbf{a_2}$ with respect to Phobos' keplerian gravity term in the point, and they correspond to [18]. In conclusion, the CR3BP does not provide an accurate approximation to describe the Mars-Phobos system's dynamics: the gravity harmonics and the orbital eccentricity of Phobos are the main orbital perturbations in proximity of the moon, and outside its Hill's SOI boundary the eccentricity becomes the dominant term, with Mars J_2 being the second largest.

2.4. Radiation Environment

The microgravity that characterizes the space environment has important implications on the spacecraft structure and subsystems design, as well as for human crew physiological and biological effects. In particular, the ionizing part of the space radiation in the Solar System, which is not shielded by the atmosphere and magnetic field as it happens here on the Earth surface, is currently considered the most challenging engineering aspect in designing a safe manned mission in deep space [19].

The Sun's activity is variable and constituted

by gradual radiative and particle production and by impulsive particle events, the latter emission is collectively called Solar Energetic Particle Events (SEPEs): they are high-energy charged particles and they constitute the hazardous ionizing part for the organic tissues. The low-energy charged gradual particles (mainly protons and electrons) constitute a plasma flow, called the solar wind. Its interaction with the magnetic field of a planet produces the so-called Magnetosphere: this is a region where the charged particles remain trapped by the magnetic field lines, known as radiation belts, but despite they are hazardous when crossed, they provide the natural shield that protects life on the Earth's surface (in combination with the ozone layer counteracting the UV rays), satellites in LEO, and in particular the crew of the ISS, from outer space radiation. In addition to the Sun, there is a second very important radiation source in the Solar System known as Galactic Cosmic Rays (GCRs). These are gradual high-energy charged particles that originate from interstellar space.

Focusing now on the Mars-Phobos system, the Mars magnetic field is very weak, so no trapped particles (and related shielding) constitute the radiation environment for a mission following the orbit of Phobos, which is similar to a deep space environment at the Sun-Mars distance, constituted by two main sources: the protons from SEPEs and protons and alpha particles from GCRs. For applications to future manned mission to Phobos' orbital environment, we conducted an estimation analysis with the open-source SPENVIS program [20] and its dedicated model for Mars MEREM [21]. To derive an approximated figure of the gross effect of the radiation environment (without any shielding effect of the spacecraft structure) to human factors, we consider the dosimetry quantity called the Effective Dose (Ef.D., whose IS unit is the Sievert, Sv), which represents the amount of energy that the radiation deposits in $1kg$ of the material's mass, averaged through both the incoming radiation and the reference tissue compositions.

The result obtained for the gross radiation hazards for a mission in Phobos' orbit from 2010 to 2030 is Ef.D.= $1.9Sv/y$, $1.1Sv/y$ from SEPEs protons and $0.8Sv/y$ from GCRs protons and alpha particles. This should now be compared with the estimated allowable dose amount for astronauts, which is based on the recommendations of the National Council for Radiological Protection (NCRP) and is currently used by both NASA and ESA [22]. Considering the case of a 35-year old astronaut, the figure derived from our analysis, for a Martian orbital segment of one year without any structural shielding, falls inside the range 1.75-2.5Sv that indicates the maximum amount of radiation dose that such human crew could be allowed to absorb throughout the entire mission. Thus, the development of a strong shielding strategy for crewed missions is required. An interesting idea that has recently gained attention, is that a manned spacecraft during a Mars orbital mission segment could exploit Phobos as a passive radiation shield: staying in its shadowing wake would theoretically counteract the gross Ef.D. of the directional part of the SEPEs, while simply remaining close to the moon will block any incoming isotropic particles (remaining SEPEs and GCRs) as much as its bulk covers the sky. Following this idea, in this paper we investigate possible orbits to be used also for shielding purposes about Phobos. However, some additional albedo effects (of the GCRs neutrons) could be relevant, and also covering the field of view of the Sun has not been proved to be relevant, as the scattering effect of the particles along the Heliosphere's lines of field is still a current topic of research [23].

2.5. Lighting Conditions

In this subsection we analyze and quantify the lighting conditions around Phobos, in particular we describe the shadowing opportunities that could exploit Phobos as a natural shield against the directional solar radiation.

Since we are interested in Phobos' neighborhood, the analysis is conducted in the CR3BP reference frame but centered in Phobos, aligned with its BCBF frame. The kinematics must now consider also the motion of the Sun in this frame, using a restricted four-body model to evaluate the field of view of the Sun over time for points around Phobos. In particular, the Mars heliocentric orbit is the second most elliptic among the Solar System planets, and Phobos' orbit is equatorial, with the resulting orbital plane inclined with respect to its ecliptic plane by Mars' rotational tilt $\theta_M = 25.19°$. The resulting Sun adimensionalized position vector in the CR3BP frame rotates clockwise with an angular velocity equal to the difference between Phobos and Mars revolution rates (dominated by the first), with a fixed declination in the range $[-\theta_M, \theta_M]$ according to the seasonal phase of Mars (seasons of Phobos correspond chronologically with Mars' ones, so we refer to them without any distinction).

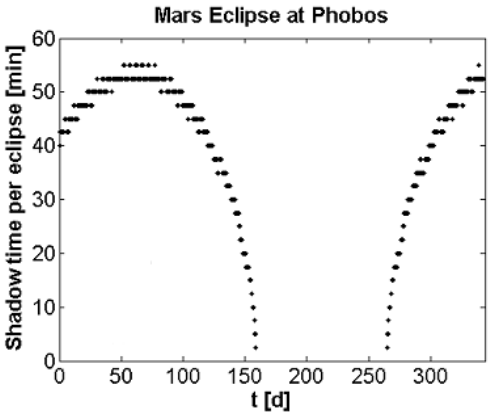

Figure 4: **Sun-Mars eclipse at Phobos.** Eclipse times are defined for a single eclipse during one Phobos' rotation.

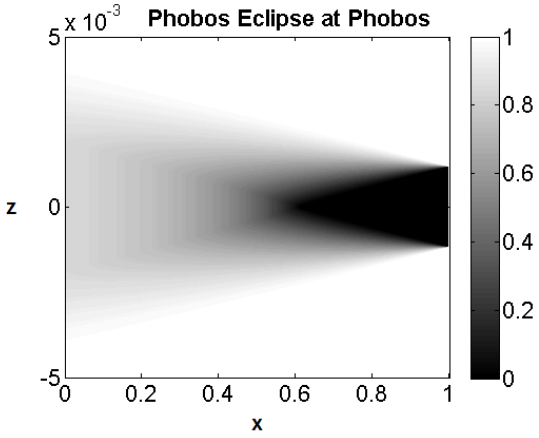

Figure 5: **Sun-Phobos eclipse.** Light function of the dual-cone model. CR3BP frame, Sun in superior conjunction.

The analysis of the shadowing effects in this system is undertaken using eclipse modeling, which is to derive the zones of light and shadow produced by a shadowing central body $\oplus$ when illuminated by a radiating body $\odot$, described by a scalar light function field $L_{\odot,\oplus}$, ranging from 0 to 1 to express the ratio of incident light with respect to the complete light case (the shadow function S is the 1-complement of L). The most accurate dual-cone model in Fig.5 is able to discriminate positions of complete light ($L = 1$), complete shadow ($L = 0$) inside a conic wake, and penumbra ($L \in (0, 1)$). When the positions of interest are very close to $\oplus$ and when there is a great difference between the two bodies dimensions, the analysis could be simplified to a cylindric model, where the shadowing wake is cylindrical and the transition zones of penumbra

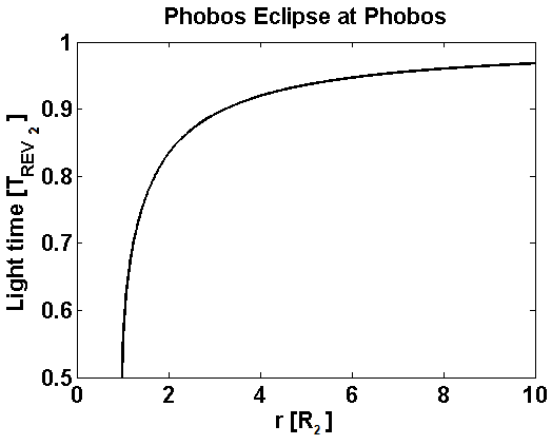

Figure 6: **Sun-Phobos eclipse.** Mean light function versus distance from Phobos on the anti-Sun surface of motion.

vanish, so positions are only in complete light or shadow.

The approach we used is to analyze the shadowing effect of each couple of bodies. The first case is the Sun-Mars couple. Here we are interested in the value of L at the Phobos location. Using the dual-cone model the Phobos SOI is a near and small domain in the Mars shadowing wake, therefore the analysis of this couple is undertaken with the cylindric model. The Sun-Mars L_1 over time at Phobos has a small-period variation due to the fast revolution of Phobos, and a long-period variation due to Mars' revolution; the latter motion inclines the Mars shadow cone with respect to the 3BP orbital plane, such that during winter and summer Phobos is constantly in light, without Martian eclipses: due to Mars high eccentricity, seasons are unequal, with the Northern Hemisphere of Mars and Phobos experiencing a summer longer than that occurring in the South. Fig.4 summarizes the outcomes: the maximum eclipse time at the equinoxes is $54min$, corresponding to 12% of Phobos daytime; summer's total light period is about 164 days (3 Martian months), and in the winter this is about 110 days (2 months).

The second case is the shadowing effect provided by the Sun-Phobos couple. For this preliminary analysis, the mean spherical shape of Phobos is considered. Like for the Sun-Mars L, the cylindric approximation is suitable in proximity of Phobos, but now the Sun-Phobos L_2 is a time-variant 3D field: since this is axially symmetric along their rotating conjunction line, it is defined on the half-plane whose reference axis is such line. The mean

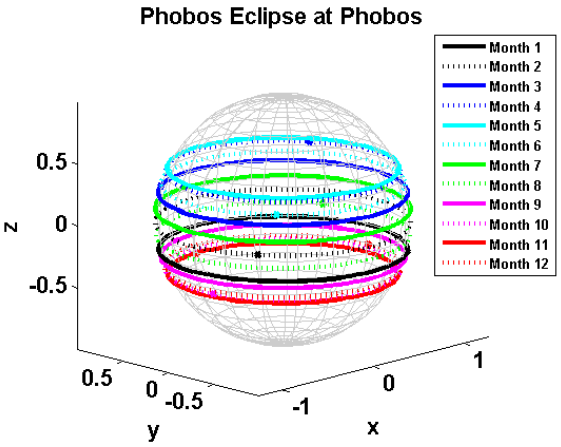

Figure 7: **Sun-Mars-Phobos eclipse.** Anti-Sun daily orbit in spherical coordinates around Phobos over the Martian year.

integral value $\bar{L}_2$ along one Phobos' revolution period, for a given distance to Phobos, is minimum on the surface of motion where the conjunction line between the anti-Sun and Phobos revolves, shortly becoming 1 in points out of the surface: such minimum value rapidly increases with the distance from Phobos. This is shown in Fig.6: from $\bar{L} = 50\%$ at the body's surface, $\bar{L} = 78\%$ at the SOI's boundary, $\bar{L} = 83\%$ at 2 Phobos radii.

The last shadowing case is the Mars-Phobos couple. Since the radiation of Mars (without the albedo) is inside the IR spectra, such eclipse analysis is neglected because it brings little variation to the radiation hazards that we aim to reduce (MRP flux at Phobos is two orders of magnitude lower than SRP one).

The conclusion of the analysis of the shadowing effects is now obtained combining the previous single couples into the system of three massive bodies of the R4BP, focusing the analysis in Phobos' neighborhood. The Sun-Mars L_1 is simply a scalar value along the Martian year, while the Sun-Phobos L_2 field must now consider the real dynamics of the Sun, which is moving in the CR3BP frame of reference (actually we are going to consider the direction of the anti-Sun $\odot'$ because it is more immediate to relate it with the position of the shadowing wake of Phobos). Fig.7 shows a complete orbit of the anti-Sun for every season: the cylindrical shadowing wake of Phobos revolves around its spin axis with the period of Phobos, and varies its inclination with the season $\theta_{\odot'} \in [-\theta_M, \theta_M]$ (when the anti-Sun is in the Northern Hemisphere, we are in winter). Besides, Phobos realm is in complete shadow when a Martian eclipse occurs, which is when the anti-Sun is close to the positive direction of the 3BP x-axis frame, enduring from a maximum at the equinoxes to zero during summer and winter.

The approach taken to compute the light function of the R4BP model in proximity of Phobos follows the following procedure. First we compute the Sun-Phobos mean integral field $\bar{L}_2$ along one Phobos' revolution for different seasons. Due to the axial-symmetry of L, the desired integration of a 3D field along time is simplified to an uncoupled 1D integral in polar coordinates, and it is also symmetrical along the spin axis. For the particular case of a cylindrical light function, the analytical solution is derived in Eq.4, where r and φ are the radial distance and declination over the equatorial plane of the point considered [24], and R is Phobos' radius.

$$\begin{cases} \gamma = \frac{\pi}{2} - \theta_{\odot'} \\ \theta = \varphi - \theta_{\odot'} \\ \alpha\left(R/r, \theta\right) = \mathrm{Re}\left\{\arccos\left(\frac{\cos \arcsin(R/r)}{\sin(\gamma-\theta)\sin\gamma} - \frac{1}{\tan(\gamma-\theta)\tan\gamma}\right)\right\} \end{cases} \tag{3}$$

$$\bar{L}_2\left(r, \varphi\right) = 1 - \tfrac{1}{\pi}\left|\alpha\left(R/r, \theta\right) - \alpha\left(0, \theta\right)\right| \tag{4}$$

Further averaging the daily $\bar{L}_2$ along the seasons of the Martian year is then straightforward.

But before doing this, the second step is to extend the Sun-Phobos daily $\bar{L}_2$ to take into consideration the correction due to the Sun-Mars $\bar{L}_1$ at the current day previously derived, to obtain the aimed Sun-Mars-Phobos mean 3D light field $\bar{L}_{12}$ that models a coupled 3B eclipse. This is far from an easy operation, but since both 2B light fields are cylindrical, and their shadowing wakes have very different dimensions, the instantaneous combined L_{12} around Phobos is the logical conjunction $\wedge$ of the two single instantaneous light functions, which results in their product: $L_{12} = L_1 \wedge L_2 = L_1 L_2$. This allows us to compute the sought mean integral field $\bar{L}_{12}$ over one Phobos' revolution with only the information of the two single daily values $\bar{L}_1$ and $\bar{L}_2$, with the deal of introducing a further variable ψ, which is the right ascension with respect to Phobos of the point analyzed. This is described in Eq.5. $\bar{L}_2$ is axially symmetric along the spin axis, being the same for points with same φ: they have the same profile $L_2(t)$, but shifted along time for different ψ. Therefore the integral of the product $L_1 L_2$

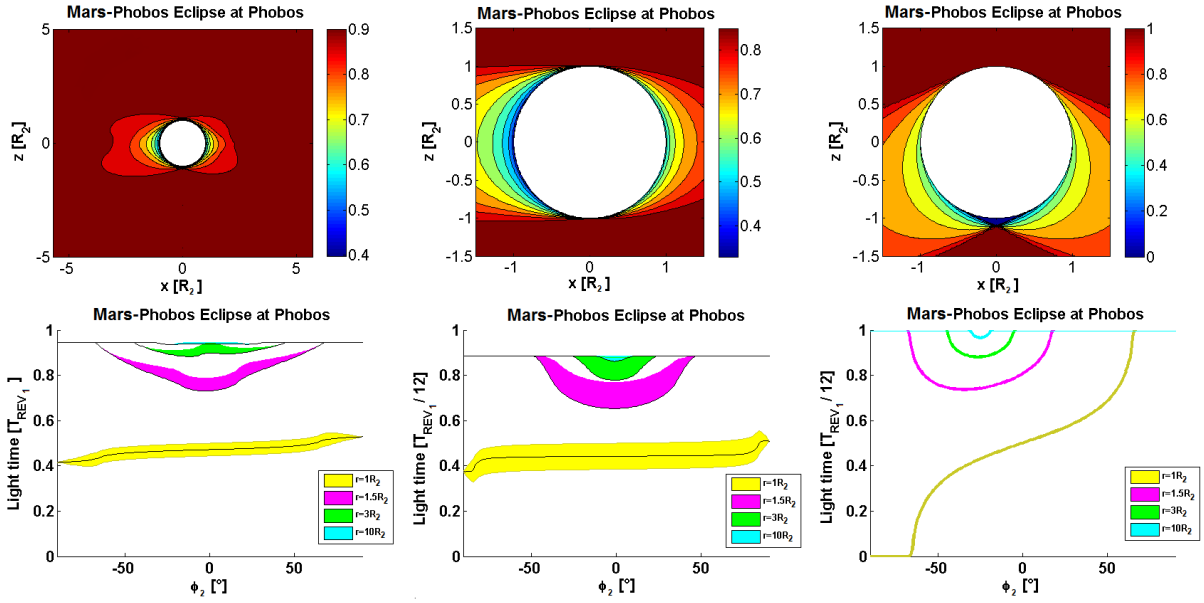

Figure 8: **Lighting conditions around Phobos.** On the top, light field around Phobos in the radial-vertical plane of the CR3BP frame, averaged over a year, a spring equinox month, a summer solstice month. On the bottom, corresponding plots function of the declination, evaluated for some radial distances, show also right ascension dependency, where upper/lower border of the filled area is for points in superior/inferior conjunction positions, and black line is for points in quadrature.

produces a different $\bar{L}_{12}$, expressed by the correction term $\Delta t/T$ which is the percentage of time in one Phobos' revolution period T such that L_1 is in shadow and L_2 is in light. This correction will be maximum for points facing Mars and minimum for those on the other side as presented in Eq.6, while the values in quadrature become closer to the maximum as far as the radial distance increases.

$$\begin{aligned} \bar{L}_{12}(r,\varphi,\psi) &= \tfrac{1}{T}\int_0^T L_1(t)\, L_2(r,\varphi,\psi,t)\, dt = \\ &= \bar{L}_2(r,\varphi) - \tfrac{\Delta t_{L_1=0\wedge L_2=1}}{T}\left(\bar{L}_1, \bar{L}_2, \psi\right) \end{aligned} \tag{5}$$

$$\begin{cases} \min\limits_{\psi} \bar{L}_{12} = \bar{L}_{12}(r,\varphi,\pi) = \bar{L}_2(r,\varphi) - \min\left(\bar{S}_1, 1-\bar{S}_2(r,\varphi)\right) \\ \max\limits_{\psi} \bar{L}_{12} = \bar{L}_{12}(r,\varphi,0) = \bar{L}_2(r,\varphi) - \max\left(0, \bar{S}_1 - \bar{S}_2(r,\varphi)\right) \end{cases} \tag{6}$$

To interpret the results in Fig.8 we should distinguish seasonal and yearly averaging. The seasonal tilt inclines the shadow wake, so complete light and one cone of complete shadow appear in the Phobos polar regions: the cone's maximum altitude, using a mean ellipsoidal model for Phobos shape, is of $1.4km$. Instead during spring and fall, no complete shadow zones are present, and the minimal daily $\bar{L}$ at the day of equinoxes is 38% along the sub-Mars meridian onto the surface of the moon (this without considering its orography and morphology). Considering now the annual $\bar{L}$, yearly averaging drastically increases the light conditions. Due to Mars' eccentricity, Southern regions experience more shadow time than the upper counterpart; due to the Martian eclipses, points in-between Mars and Phobos and close to the moon experience more shadow time per annum.

In conclusion, this analysis provides the lighting conditions for a spacecraft orbiting Phobos. Focusing on the shadowing opportunities, a fixed observation point in the 3BP frame could provide relevant reduction of the field of view of the Sun for long-period station-keeping only if it is inside the SOI and onto the equatorial plane, and pointing Mars; instead, a shorter period could provide continuous shadowing opportunities for points over the poles during the solstice seasons, in particular inside the Southern polar cone during summer. Instead, for middle seasons the minimum of the light field moves towards lower latitudes, and relevant reduction of the Sun field of view is obtained only very close to the surface. Therefore during equinoctial or long observation periods, the lighting conditions around Phobos are close to experience continuous light, up to 88% due to the unavoidable Martian eclipses. Suitable shadowing exploitation could be obtained

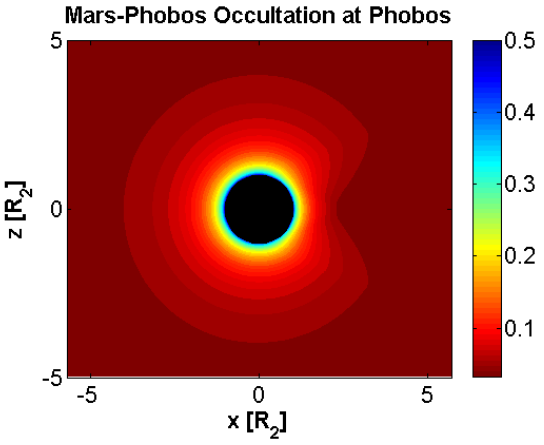

Figure 9: **Sky occultation around Phobos.** Occultation field around Phobos in the radial-vertical plane of the CR3BP frame.

only using orbits that track the daily anti-Sun path, such a vertical displaced circular orbit around the spin axis. We acknowledge that a complete shadowing is not possible with current technologies, because a spacecraft requires sunlight for the electrical power generation from the solar arrays, with the solar flux decreasing with the distance from the Sun.

2.6. Sky Occultation

In this subsection we consider the possible exploitation of Phobos as a natural shield against the isotropic cosmic rays (SEPEs and GCRs): the idea is that the incoming radiation on a spacecraft is lowered proportionally to the filling fraction in the sky of the apparent size of the body's bulk, as seen by the spacecraft's location. In astronomy, when a body is totally or partially hidden by the bulk of another one that passes between it and the observer, we speak about occultations or transits. Since in this case the hidden body is the total background sky, in this paper we refer to this action as sky occultation.

A point-like observer sees an object with an apparent shape that corresponds to the area that it covers on a sphere centered on the observer, and radius equal to their distance. In 3D geometry, the area subtends the 2D solid angle Ω on the unit sphere (whose IS unit is the steradian, sr), and the total spherical surface has $\Omega = 4\pi sr$. For a general body placed at distance d from the observer,

$$\Omega = \iint_{0,0}^{2\pi,\pi} M(\vartheta,\phi)\sin\vartheta d\vartheta d\phi \qquad (7)$$

where M is the mask function of the body. This is a binary function of the polar and azimuthal spherical coordinates ϑ and ϕ centered on the observer, whose value is 1 or 0 if the related direction from the observer intersects or not the body: it represents the apparent shape of the body on the unit sphere. The ratio with $4\pi sr$ represents the filling fraction of the body with respect to the background.

The occulting bodies in our case are Mars and Phobos, while the Sun is neglected because it is very small as seen from Phobos. The approach is similar to the one undertaken for the lighting conditions, defining an occultation function field $O_{\oplus}$ which represents the bulk/sky filling fraction of the occulting body $\oplus$. This analysis is easier because in the CR3BP frame Mars and Phobos are fixed, and their O does not depend on time. For a first analysis, we consider the mean spherical shapes for the two bodies, of radius R. In this case, the occulting body fills a spherical cap on the unit sphere, with apparent angular radius $\alpha = \arcsin(R/d)$, and $O = \frac{1-\cos\alpha}{2}$, which is spherically-symmetric. First we consider the occultation of Mars, at the Phobos location, since the region of interest is small: the result is $O_1 = 3.4\%$. Second we consider the occultation of Phobos, which depends only from the radial distance from the body. This function starts from $O_2 = 50\%$ on the surface (astronauts staying inside of a deep crater would be shielded also laterally by the mountain ridge), and then decreases rapidly: $O_2 = 13\%$ at the SOI's boundary, $O_2 = 7\%$ at 2 Phobos radii. The conclusion of the analysis of the sky occultation is obtained combining the previous single effects. This requires to determine if the apparent shapes of the two bodies' bulks intersect, and how much they overlap: such axially-symmetric 3D field corresponds to the light function of the Mars-Phobos couple $L_{1,2}$ that we avoided to compute in the previous lighting conditions analysis, but we do need here. In particular, this light function must be computed with the accurate dual-cone model, since due to the proximity of Mars, the shadow cone vertex of Phobos is located only at 2.77 Phobos radii in the anti-Mars direction, therefore its inclination inside the SOI is not negligible. The resulting 2B combined occultation function is $O_{12} = O_2 + L_{1,2}O_1$ and it is shown in Fig.9.

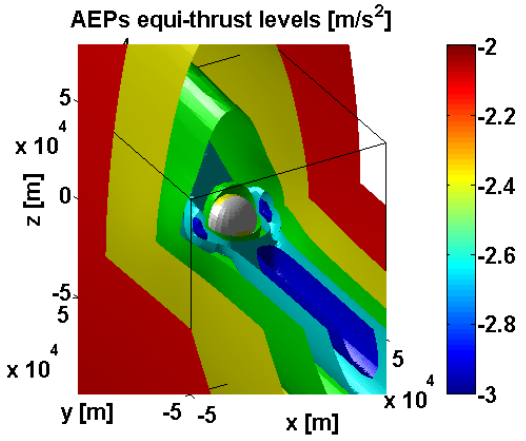

Figure 10: **AEPs of the Mars-Phobos system.** Isosurfaces slices of propulsive acceleration magnitude (logarithmic scale).

This analysis highlighted that mild but relevant reduction of the isotropic SEPEs and GCRs by using the bulk of Phobos to occult part of the celestial sphere is obtained inside the SOI of the moon. Besides, points on Mars' side and over the poles experience an additional but small reduction due to the occultation of Mars. Orbits that remain inside the Phobos' SOI are therefore suitable to enhance the radiation protection of the spacecraft by exploiting Phobos' bulk as a passive radiation shield.

3. Hovering Points around Phobos

A simple trajectory for a mission around Phobos is provided by maintaining a fixed position with respect to its BCBF frame: due to the small μ, this is similar to a Martian keplerian orbit close to Phobos, analogous to the Trailing/Leading configurations used in Formation Flying [25]. The analysis of these trajectories is undertaken adding a constant propulsive acceleration $\mathbf{a_P}$ to the equations of motion of the CR3BP, which will be referred CR3BP-CA. The aim of the hovering in a point is therefore to counteract the natural acceleration of the CR3BP, and thus leading to an Artificial Equilibrium Point (AEP).

$$\mathbf{a_P} = \mathbf{a_A} - \mathbf{a_G} \tag{8}$$

Recall from [25] that SEP Hall/ion thrusters operate roughly in the medium range of $0.01mN$-$0.1N$, new generation FEEP and colloid thrusters provide low-thrust down to $1\mu N$ scale, and electrothermal propulsion (resistojets and arcjets) supplies the higher ranges up to $1N$, but the levels of propulsive acceleration must be scaled accordingly to the mass of the spacecraft ($100kg$ for a medium-size interplanetary satellite, 100 times larger for a big manned module). Fig.10 presents the isosurfaces of the thrusting acceleration level required to hover around Phobos: as far as the propulsion grows, AEPs could be further displaced from the natural equilibrium points of the CR3BP, which are the three collinear libration points (LPs) aligned with the two bodies (two close to the secondary, L_1 in inferior and L_2 in superior conjunction, and L_3 in opposition), and the two equilateral LPs L_4 and L_5 equidistant from them in the two quadrature configurations; in particular, the cis/trans couple of LPs L_{1-2} is located on the boundary of the Hill's SOI of the secondary, at an altitude of $3.5km$ from Phobos. Despite this proximity, the thrust level required to establish an AEP displacing a collinear LP is very demanding. Instead, displacing the equilateral LPs L_{4-5} is very cheap and effective, arriving close to Phobos along the y-axis still with small values of thrust; on the other end, establishing AEPs over polar regions requires high thrust levels.

The next step in the hovering analysis is to look for the stability of the AEPs analyzing the linearized CR3BP-CA: since the propulsive acceleration is constant, the linearized system coincides with the one of the CR3BP. The 3D stability requires the computation of the eigenvalues λ of the 6D linearized state-matrix, that contains the 3D Hessian matrix H_u of the gravity potential evaluated at the current AEP. Due to the sparse structure within the state-matrix, it is possible to derive a condensed analytical expression of the three couples of opposite eigenvalues in terms of the three scalar invariants of the hessian matrix (which is symmetric) I_1, I_2, and I_3. To do so, we introduce some coefficients: A, B and D are strictly real scalars by definition, instead C is complex. The expression of the three couples of eigenvalues is expressed in a convenient symmetrical form in the complex field in Eq.10.

$$\begin{cases} A = \frac{I_1 - 2}{3} \\ B = \frac{I_2 + I_1 + 1 - H_{u3,3}}{3} - A^2 \\ C = \sqrt[3]{\sqrt[2]{D^2 + B^3} + D} \\ D = \frac{I_3 + I_2 - H_{u1,1} H_{u2,2} + H_{u1,2}^2 + H_{u3,3}}{2} - 3\frac{AB}{2} - \frac{A^3}{2} \end{cases} \tag{9}$$

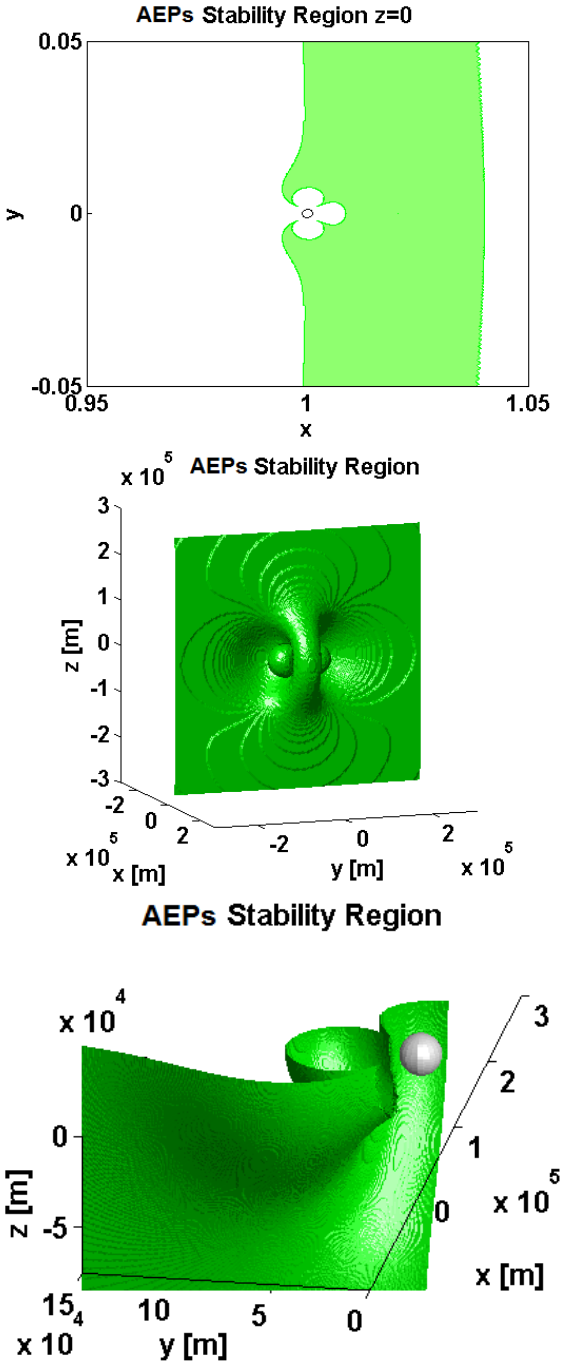

Figure 11: **AEPs of the Mars-Phobos system.** On the top, planar stability region (in green) around Phobos. Following figures show the inner boundary of the 3D stability region around Phobos (in the last picture, only one half of the lower hemisphere is represented to visualize Phobos mean sphere).

$$\lambda = \pm\sqrt{A + \frac{B}{C}e^{(\pi-\theta)i} + Ce^{\theta i}},\ \theta = 0, \pm 2\pi/3 \tag{10}$$

The linear Lyapunov marginal stability for the AEP requires all the eigenvalues to be purely imaginary, which is their squares to be real and negative. To solve these two constraints, we use the magnitude-phase notation for $C = |C|e^{\theta_C i}$: the first constraint is satisfied by one simple relationship between B and C, which is the necessary condition for real eigenvalues. Using this, Eq.10 could be rewritten in a compact way where the six solutions derive from the same definitions of C as a cubic root of Eq.9. The second stability constraint consists of one simple inequality, which considers the algebraic root of C with maximum real part (there is at least one that is strictly positive-definite).

$$\lambda = \pm\sqrt{A + 2\,|C|\cos\left(\theta_C + \theta\right)},\ \theta = 0, \pm 2\pi/3 \tag{11}$$

$$\begin{cases} B = -|C|^2 \\ A + 2\mathrm{maxRe}\left\{C\right\} < 0 \end{cases} \tag{12}$$

This approach extends the result obtained for only the planar case of the CR3BP-CA of [26]. For the Mars-Phobos system, the 3D stability region is made of three realms: one central ring, and two symmetric half hyperbolic coronas placed at very high out-of-plane altitudes. More interesting as presented in Fig.11, the inner surface of the ring is distorted in proximity to the second massive body leaving outside the body's SOI. The planar stability region in the orbital plane is a thin corona extending along the Mars-Phobos orbital distance, that comprises the equilateral LPs and cuts off the three collinear LPs, and in proximity of the secondary body, the inner stability region boundary is distorted to represent a three-leaves clover: this corresponds to the outcome in [27]. Recall that this is the linearized stability region, which for the case of marginal stability encountered by the AEPs does not assure stability in the original CR3BP-CA. However, it has been proved by analysis of higher order terms that the AEPs of the linearized stability region are also stable in the full nonlinear dynamics apart from singular cases that lie on co-1D domains of the stability region, where resonance effects are present [26].

If we compare the stability region with the equi-thrust curves in the orbital plane, it can be seen

that the planar stability boundary is not too far from Phobos, starting from $25km$ (in the petal-head connection border, requiring $1.9mm/s^2$), $71km$ (on the tip of the top and down leaves, $0.4mm/s^2$) or $81km$ (along the x-axis, $12mm/s^2$) and arriving to $400km$ (along the x-axis, where the outer boundary lies). Therefore six attractive positions for medium distance observation of Phobos are identified: four minimum-distance AEPs at $25km$, and two minimum-control AEPs with $0.4mm/s^2$, all obtained by the displacement of the equilateral LPs and affordable by current light electric thrusters. Further trailing/leading orbits around Mars provide attractive cheap, stable, in-light fixed positions with respect to Phobos at long distances from the moon. All the AEPs available with a low-thrust level are not stable near the collinear LPs, and AEPs closer to Phobos, used to maximize the shadowing time and the sky occultation ratio, or perform short dedicated operations, are feasible only with heavy or multiple thrusters, and must take into consideration in the model also the complete inhomogeneous gravity of Phobos: this increases the precision, frequency and computational load of the GNC subsystem. Regarding the 3D boundary, it is possible to have stable AEPs above the poles of Phobos, but at a great distance (from $250km$ to $1400km$) and with high thrust.

4. Vertical-Displaced Circular Orbits around Phobos

The AEPs computed in the previous section are a fixed solution in the rotating frame of the CR3BP. It is possible to further generalize the concept, which is to look at the dynamics in a general uniformly rotating frame, and find the related AEPs. In the usual CR3BP, such solution results in a circular orbit around a reference axis, which in our case will be Phobos' vertical axis: it is called a Vertical Displaced Circular Orbit (VDCO). Therefore, if the angular velocity of the VDCO is opposite to the one of the Phobos revolution, and the declination of the VDCO is opposite to the one of the Sun, a spacecraft along this orbit experiences constant light or shadow conditions during a season, realizing a Sun-Synchronous (SS) seasonal orbit whose β-angle performance (expressing the mean time in light) is set by the choice of the initial phase along the VDCO with respect to the Sun. In particular, for continuous shadowing ($\beta = 0$) the spacecraft tracks the position of the anti-Sun moving clockwise around

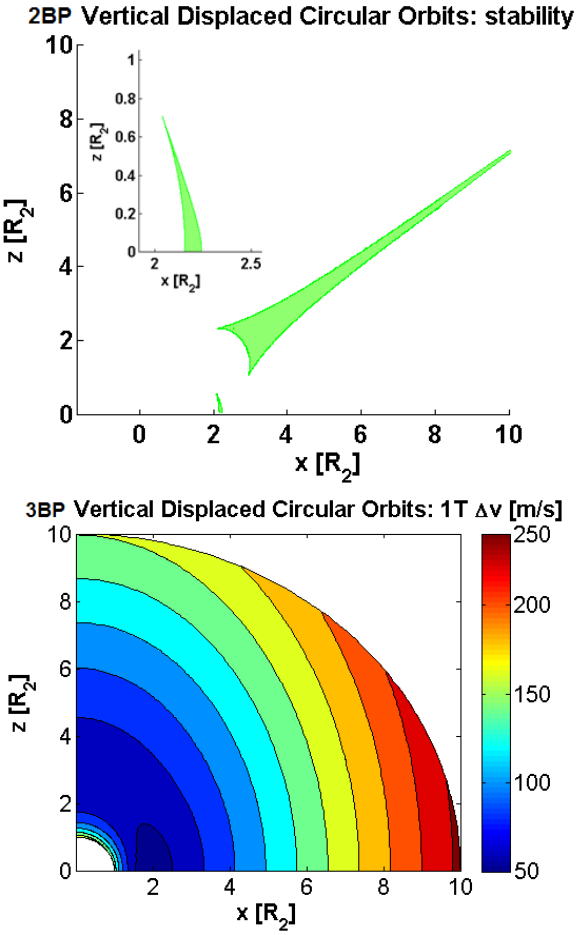

Figure 12: **SS-VDCOs around Phobos.** AEPs in the x-z plane of the SS-rotating frame. On the top, linearized stability region for AEPs in the Phobos 2BP (magnification of the inner section). On the bottom, Δv for one period for AEPs in the CR3BP.

Phobos: this is expressed in Fig.7. These displaced orbits are usually highly non-keplerian: here, we are going to consider the type III orbits of [28], which have fixed period, synchronous with the Sun around Phobos, and looking to incorporate low-thrust.

The approach is to start from the 2B dynamics around Phobos in a rotating frame R, defined by Eq.1 taking $\boldsymbol{\omega}$ opposite to the Mars-Phobos mean motion and considering only the gravity of the moon. The model is axially symmetric around the vertical axis, therefore it is defined either in the positive x-z plane of the R frame, or in the polar counterpart R-δ. The SS-VDCOs are AEPs of this dynamics maintained by a constant acceleration in the rotating frame's components from Eq.8: in case of complete light or shadow applications, the dec-

lination of the AEP must be equal to the seasonal anti-Sun declination, therefore the domain of interest is $0 \leq \delta \leq \theta_M$, or $0 \leq z \leq x\tan\theta_M$. However, shadowing is provided not only by strictly pointing toward the anti-Sun, but remaining just inside the eclipse wake: using a mean ellipsoidal model for Phobos' shape, a SS equatorial circular orbit with radius 2.04 Phobos mean radii provides continuous shadow for all the Martian year.

The procedure is the same followed before for the hovering, computing the equi-thrust curves and the related linear Lyapunov stability region. There is one natural equilibrium point that corresponds to the keplerian equatorial circular orbit with a SS period achieved at the distance of $\tilde{R} = 2.16$ Phobos radii (mean altitude of $11.8km$), and no other local minima of the thrust level. The three realms of the linear stability region in Fig.12 are similar to the ones of the 3D stability region for AEPs of the CR3BP-CA, swapping the Mars-Phobos barycenter and Phobos with Phobos and the keplerian equilibria, and without the distortion of a second massive body. For planar SS circular orbits this means that orbits with radius in the interval $[\tilde{R}, \sqrt[3]{9}/2\tilde{R}]$ are linearly stable in the 2B dynamics, while stable SS-VDCOs could be obtained at higher distances with declination $\delta = 35.26°$ and high thrust.

We now look to the solution of VDCOs around Phobos in the framework of the CR3BP. The dynamics will be described in the same rotating frame R of the VDCO centered in Phobos: the equations of motion of this model are obtained from the previous one adding the time-variant gravity of Mars. Since its location is not fixed in this frame, and considering that now Phobos moves around Mars, an additional time-variant apparent acceleration must be enabled in Eq.2, $\mathbf{a_{A,T}} = \mathbf{a_{G}}_1(\mathbf{0})$, equal to the Martian gravity at the origin of the R frame. And finally, the Phobos revolution affects also the inertial reference of the R frame: since the R frame must move clockwise with respect to the Phobos BCBF frame, and now the latter is rotating in the opposite way, Eq.2 must be used with $\boldsymbol{\omega} = \mathbf{0}$. Indeed, in a short-time analysis, the Sun is approximately fixed with respect to an inertial frame centered on Phobos, therefore realizing a SS-VDCO around Phobos corresponds in maintaining an inertial fixed point dragged along the Mars-Phobos orbit.

The system is no longer axially symmetric, but the required acceleration is periodic so we consider the maximum level of the thrust profile and its cost over one period, defined by the Δv and presented in Fig.12. Being the problem time-variant, no natural equilibria are available. The max thrust level for a $100kg$ spacecraft at small-medium distances from Phobos is affordable only with high thrusters. The minimum cost still happens in a region close to 2 Phobos radii, up to the maximum Sun's declination at the solstices, but this is large (Δv= $50m/s$) making the demand for the propulsion system very high. Besides, a linearized Floquet stability analysis of these SS-VDCOs showed us that they are highly unstable.

Following the idea of exploiting the shadow of Phobos to protect a spacecraft from directional solar radiation during the orbital station-keeping at the Mars-Phobos orbital distance, in this section we analyzed the most simple and straightforward orbits around Phobos to track the anti-Sun motion, which are the SS-VDCOs. Due to the strong influence of the Mars' third body perturbation, the SS-VDCOs around Phobos require a huge amount of fuel consumption, which is infeasible over one period. A SS-VDCO around Mars is located out of its SOI, while the cost of a SS-VDCO around Deimos at 5 mean radii ($24.0km$ of mean altitude) has resulted to be of $16m/s$ per period, and it requires lighter thrusters.

5. Libration Point Orbits and their Invariant Manifolds around Phobos

In the framework of the classical CR3BP [15], around each of the collinear LPs L_1 and L_2 there exist a central manifold characterized by families of periodic orbits (POs) (the two branches of planar and vertical Lyapunov orbits, and the two branches of Northern and Southern Halo orbits), and quasi-periodic orbits (QPOs) around them (known as Lissajous orbits). These Libration point orbits (LPOs) are highly unstable and so their natural motion needs to be computed with high precision to provide low cost tracking opportunities [15, 29, 30]. Moreover, these LPOs are separatrices of motion between transit and non-transit orbits to enter or escape from the SOI of the second massive body: the boundary of these tubes is given by the Invariant Manifolds (IMs) of the LPOs that provide the energy-efficient trajectories to minimize the fuel consumption of spacecraft for interplanetary transfer phases.

From our preliminary analysis of the dynamics in proximity of Phobos in Section 2.2, we found

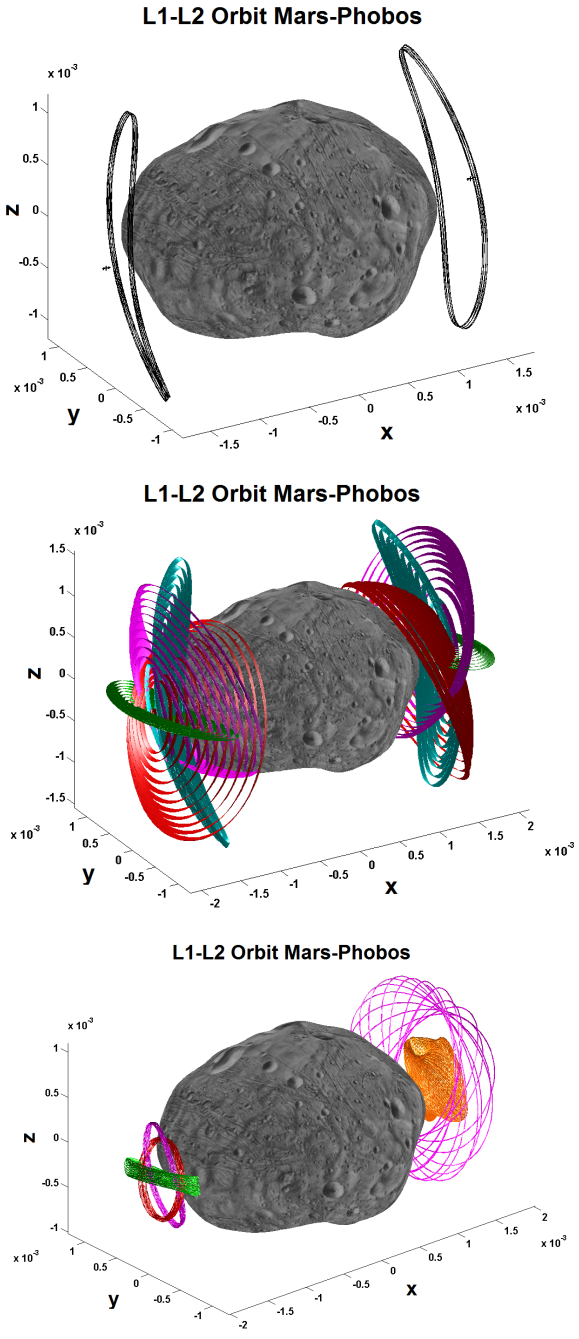

Figure 13: **LPOs in the Mars-Phobos ER3BP-GH.** On the top, the two iso-periodic families of POs around the oscillating LPs. In the center, the families of 2-tori: A (red), B (green), C (magenta), D (cyan). On the bottom, example of 3-tori of different size and width around the LPs: three medium-size QPOs of family AB (red and green with small-width, orange with high-width) and two high-width QPOs of family C (around the smallest and biggest orbits). Shape harmonics series expansion for Phobos surface.

that the altitude of the LPs moves very close to Phobos' irregular surface: in this situation, the dynamical approximation provided by the CR3BP falls short, and in particular we found in Section 2.3 that to describe the natural relative motion inside this moon's SOI, its highly inhomogeneous gravity field, and its orbital eccentricity must be taken into account. Due to their highly unstable behavior, measured by the Floquet stability indexes, the families of LPOs, computed with the classical methodologies tailored for the CR3BP, are therefore not reliable for practical applications, because their reference signal tracking will require a high station-keeping cost.

In [31]-[32] the dynamical substitutes of the LPOs were derived in a more realistic model that considers these two major orbital perturbations in proximity of Phobos. The modeling of the complete gravity field of convex bodies is provided by a spherical harmonics series expansion, known as gravity harmonics (GHs). From a previous paper [14] that collects the data obtained through Viking observations, we are provided with a model of Phobos' gravity field. The addition of the GHs in the dynamics is particulary suitable for the Mars-Phobos system because the CR3BP frame and the Phobos BCBF frame are approximately fixed with respect to each other (see Fig.2), which makes this system so unique to remain time-invariant. The equations of motion of the Mars-Phobos ER3BP-GH are derived in the Hill's frame of the Mars-Phobos orbit centered in Phobos, from Eq.1 considering the angular velocity for an elliptical orbit $\boldsymbol{\omega} = [0; 0; \sqrt[2]{G(m_1+m_2)/a^3}(1+e\cos\nu)^2/(1-e^2)^{3/2}]$ (where a and e are the semi-major axis and eccentricity of the Mars-Phobos orbit, and ν is the true anomaly of Phobos), $\mathbf{a_{A,T}} = \mathbf{a_{G1}}(\mathbf{0})$ like before for the VDCOs, and defining the gravitational potential of Phobos $u_{G,2}$ as a truncated series expansion of GHs $(J,\lambda)_{m,n}$ through Legendre polynomials $P_{n,m}$ (R is Phobos mean-volume radius):

$$u_G = \frac{Gm}{R}\sum_{n=0}^{\infty}\left(\frac{R}{r}\right)^{n+1}\sum_{m=0}^{n} J_{n,m}\cos m\left(\psi-\lambda_{n,m}\right)P_n^m\left(\cos\vartheta\right) \tag{13}$$

where the potential is defined as a function of the spherical coordinates r,ϑ,ψ of the Phobos BCBF frame, and so the gravity acceleration of Phobos in the Hill's frame is retrieved rotating back the components of the spherical gradient of the potential.

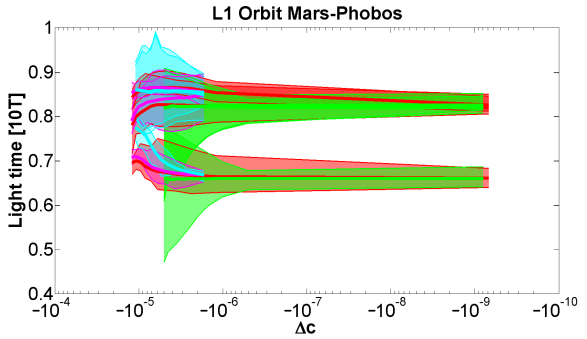

Figure 14: **LPOs lighting conditions.** Light function of the families of POs around L_1 of the CR3BP-GH (parameterized by the differential Jacobi integral with respect to L_1, in logarithmic scale), averaged over 10 PO periods, at the days of equinoxes (lower cluster) and solstices (upper cluster). Filled area spans values for different starting phases of the Sun (thick line is for mean values), where families colors are coherent with Fig.13.

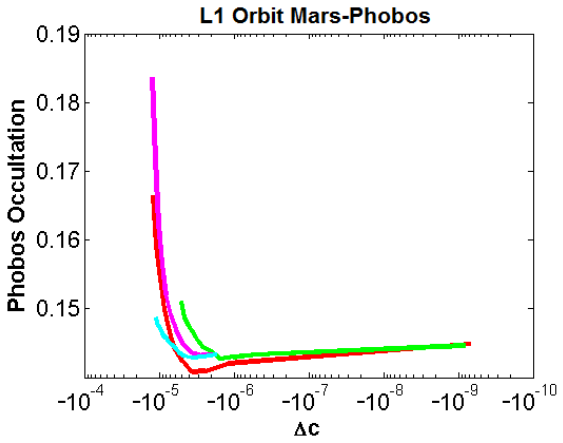

Figure 15: **LPOs occulting conditions.** Sky occultation function by the Phobos' real bulk (modeled by the shape harmonics series expansion) of the families of POs around L_1 of the CR3BP-GH (parameterized by the differential Jacobi integral with respect to L_1, in logarithmic scale), averaged over 1 PO period. Families colors are coherent with Fig.13. Additional occultation by Mars' bulk will be 3.4%.

The procedure in [31]-[32] to compute the LPOs in an ER3BP-GH makes use of the numerical continuation technique, which consists of the iteration of the classical differential corrector to compute POs and QPOs in a single dynamical system. First, we identify LPOs in the Mars-Phobos-spacecraft CR3BP using the classical tools of dynamical systems theory, and then numerically continue a parameter that incrementally increases the GHs of Phobos, to find their dynamical substitutes in the final CR3BP-GH. The introduction of the GHs produces families of POs and QPOs no longer symmetric and highly tilted and distorted from the classical case. These new LPOs are then continued again using the eccentricity as the perturbation parameter: despite the fact that the orbital eccentricity of Phobos is not particularly high, the perturbation has a significant effect on the LPOs, as an indirect effect of the long-cited collapse of the SOI towards the moon. The effect of the eccentricity makes the motion to oscillate around these solutions with a considerable amplitude of $260m$ for the proximity of Phobos.

The resulting LPOs of this improved dynamical model considerably lower the station-keeping demand exploiting the natural dynamics of the system. They are showcased in Fig.13: around each cis/trans-side of Phobos, they are constituted by the oscillating LPs and a 1-parameter family D of iso-periodic POs vertically developed with the period of Phobos revolution around Mars, three 1-parameter families A, B, and CD (made by two branches C and D) of 2-tori QPOs, and two 2-parameter families AB and C of 3-tori QPOs, all of them very close to the surface of the moon and highly unstable. Regarding the lighting conditions and surface coverage, medium-small LPOs are actually similar to close-range hovering points on the cis and trans-side of the moon, and the seasonal and annual light times are approximately the same of the ones computed in Section 2.5 (see Fig.8). Large LPOs can cover also polar and lead/trail-regions, and Fig.14 shows that if used for short operations the light time can be tuned accordingly to the Sun phase along Phobos, with the families B and D allowing to increase/decrease the mean light function up to the 15%.

In particular, due to their proximity to Phobos, the sky occultation produced by the natural LPOs is relevant, and Fig.15 shows that larger LPOs around both L_{1-2} can provide passive radiation shielding over 20%. This outcome is obtained using a high order shape harmonics model [31]-[32] for Phobos' bulk. Using Mars' bulk to provide the same shielding factor would require a low Martian orbit's altitude under $850km$, while LPOs around Deimos are too distant from the body to provide relevant natural shielding.

Since the orbits are close to Phobos, no homo-

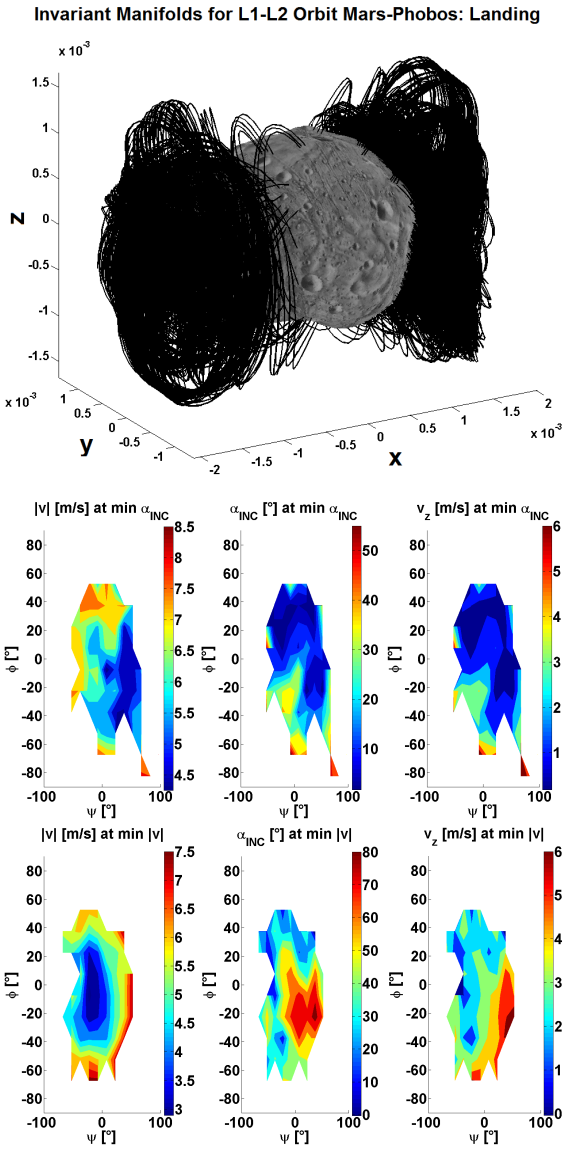

Figure 16: **IMs of the LPOs in the Mars-Phobos ER3BP-GH.** On the top, inside branch of the tube of unstable IMs from the families of 3-tori LPOs. In the center, related performances of the trajectories that provide the min incidence at the touch-down from the family AB of L_1 as a function of the longitude and latitude of the landing site on Phobos surface modeled through shape harmonics series expansion: landing velocity modulus, angle of incidence, downward vertical velocity. On the bottom, performances of the stable IMs of the same family that provide the min velocity total magnitude at the launch.

clinic nor heteroclinic connections[4] are available to naturally move around it, but the IMs of these LPOs could be exploited as natural landing or take-off gateways to and from the surface of Phobos. In particular, as presented in Fig.16, the inside branch of the IMs has been computed and a related performance analysis has shown that high-efficient natural tangential landing paths and low escape velocity injections (far less than the 2B Δv value of $11m/s$) are available for a region of topographical collinear-faced sites on Phobos. These trajectories have the potential to be exploited for future sample-and-return missions to this moon, where free-fall is required to avoid contamination of the sample's soil by the exhaust plume of the thrusters or rockets' nozzle.

5.1. Artificial LPOs and their IMs around Phobos

The natural LPOs computed in the ER3BP-GH around Phobos are investigated in the framework of the addition of a constant acceleration representing SEP. The idea is the same used in Section 3 for hovering points: here we focus on the artificial orbits around the displaced L_{1-2}. Since we found before, computing the dynamical substitutes of the natural LPOs in the ER3BP-GH, that the effects of the GHs and the eccentricity act in a different way, with the first responsible for the change in position, shape and orientation of the LPOs, and the second causing the motion to oscillate around them, to undertake an immediate analysis of the advantages and opportunities provided by the low-thrust propulsion, only the periodic artificial LPOs are derived by numerical continuation from the families of the POs of the CR3BP-GH, since they provide the backbone of both the QPOs in the same dynamical model and the QPOs in the ER3BP-GH.

The numerical continuation is undertaken increasing the constant acceleration magnitude, with the same differential approach for the differential corrector used for computing the POs from CR3BP to CR3BP-GH in [31]-[32]: the difference is that the dimension of the parameters of the problem is now higher, since it depends also on the orientation of the thrust vector; therefore, the analysis is undertaken six times to consider thrust directions along all coordinated axes $\pm\hat{\mathbf{x}}$, $\pm\hat{\mathbf{y}}$, and $\pm\hat{\mathbf{z}}$. Fig.17

[4]They are natural connections of IMs of orbits around the same or different equilibrium points in nonlinear systems [15].

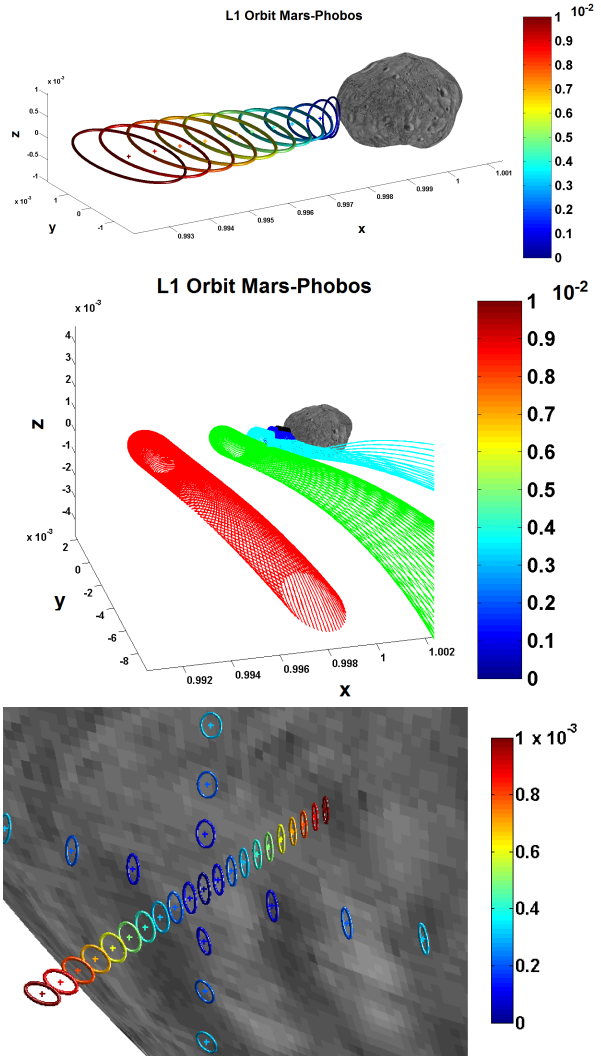

Figure 17: **Artificial LPOs and their IMs with constant acceleration in the Mars-Phobos CR3BP-GH.** First two graphs show the example of one natural medium-size periodic LPO of the family A around L_1 and the trajectories (propagation time of 2 LPO periods) of the inner branch of its unstable IM, both modified by different levels of constant acceleration magnitude (m/s^2) along the direction $+\hat{\mathbf{x}}$ (crosses represent the current LP). On the bottom, example of a small periodic LPO of the family A around L_1 with different levels of constant acceleration magnitude (m/s^2), along all coordinate axes directions.

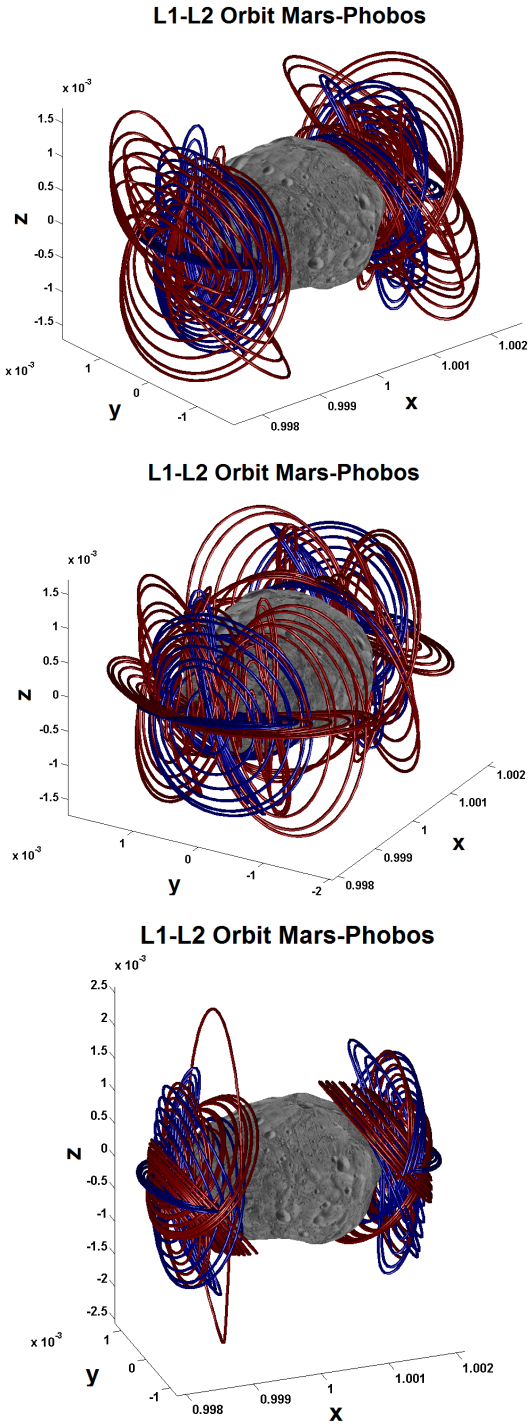

Figure 18: **Periodic LPOs in the Mars-Phobos CR3BP-GH-CA.** Summary of the POs (brown) obtained by displacement of the four families of POs around each LP of the C3BP-GH (blue) with constant acceleration ($1mm/s^2$) along all coordinate axes directions (on the top directions $\pm\hat{\mathbf{x}}$, in the center directions $\pm\hat{\mathbf{y}}$, on the bottom directions $\pm\hat{\mathbf{z}}$). Phobos shape harmonics model.

shows some examples of the effects that the addition of a constant acceleration produces on the natural LPOs, and Fig.18 showcases the resulting families of POs in the Mars-Phobos CR3BP-GH-CA along all the thrusting coordinate directions. In particular, thrusting away from Phobos moves the LPOs closer to the moon, without great changes in the shape and orientation of larger orbits even with high thrust. On the contrary, thrusting towards Phobos moves the orbits further from the moon, and as the thrust level increases the effect of the GHs rapidly decreases and the LPOs tend to become similar to the families of the classical CR3BP. The effect of the thrust along the other two coordinates axes is more complicated: the manifold moves accordingly to the thrust direction, with the displacement of the artificial LP moving in accordance to the equi-thrust surfaces computed before in Fig.10; thrust in tangential direction maintains the shape of families B and C, while the families D are similar to vertical Lyapunov orbits, and the families A are highly distorted; high thrust in the vertical direction greatly modifies the manifold, since only two families of POs are now present, one similar to the Halo orbits (Southern for $+\hat{\mathbf{z}}$) and the other distorted and perfectly lying on the y-z plane.

The addition of a constant acceleration around Phobos has revealed some interesting mission opportunities. First, Fig.19 shows that the effect on the period of the POs (the numerical continuation is undertaken with a fixed differential energy constraint) is quite sensitive: in particular, since the dimension of the manifold of the LPOs is small due to the proximity of Phobos, the range of periods of the natural LPOs is limited, and the addition of constant low thrust allows cheap artificial LPOs to be obtained with period in 2:1 resonance with the orbital period of Phobos around Mars. This means that they remain periodic also in the elliptical real scenario, which could be an advantage for designing the insertion manoeuvers between the mission segments. Second, the addition of this simple thrust profile also affects the stability properties of the POs: despite the LPOs remain unstable, the Floquet instability index could be massively lowered with the thrust required to displace the LP far from Phobos. This has a great impact on the frequency demand for the GNC subsystem, reducing the duty cycle up to the 25% for artificial LPOs displaced at an altitude over $60km$ from Phobos along the Mars-Phobos radial. In particular, we see in Fig.19 that

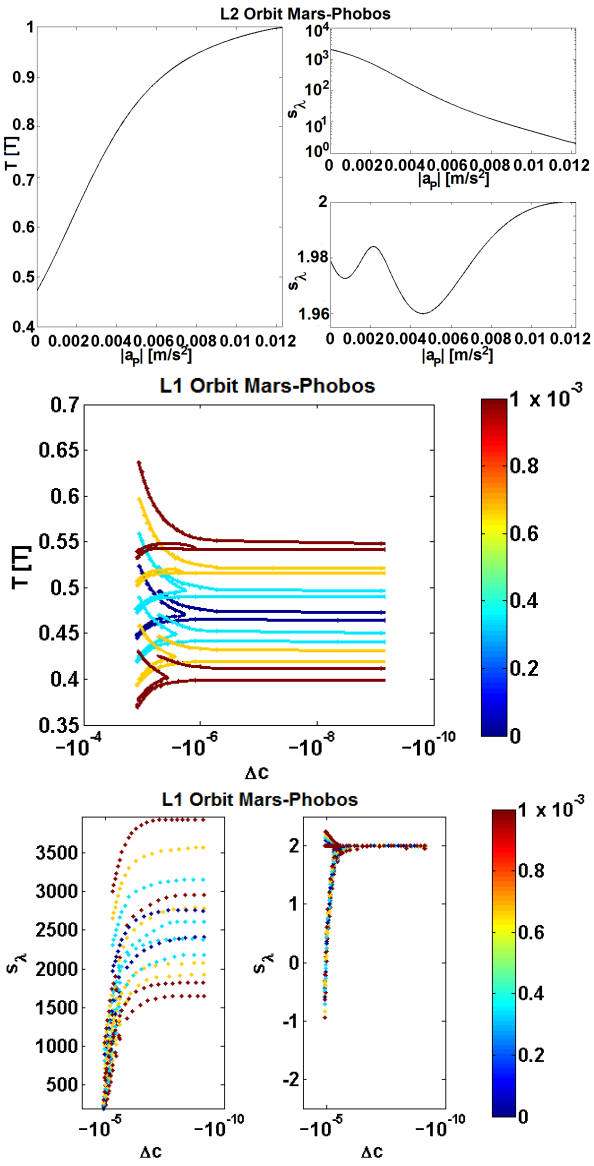

Figure 19: **Periodic LPOs in the Mars-Phobos CR3BP-GH-CA.** On the top, example of one natural medium-size periodic LPO of the family A around L_2 modified by different levels of constant acceleration magnitude along the direction $-\hat{\mathbf{x}}$: period and stability properties (stability indexes of the two non-unit couples of eigenvalues of the monodromy matrix). Following graph shows the characteristic curves of the same properties for all the four families of POs around L_1 with different constant acceleration magnitude (m/s^2) along directions $\pm\hat{\mathbf{x}}$.

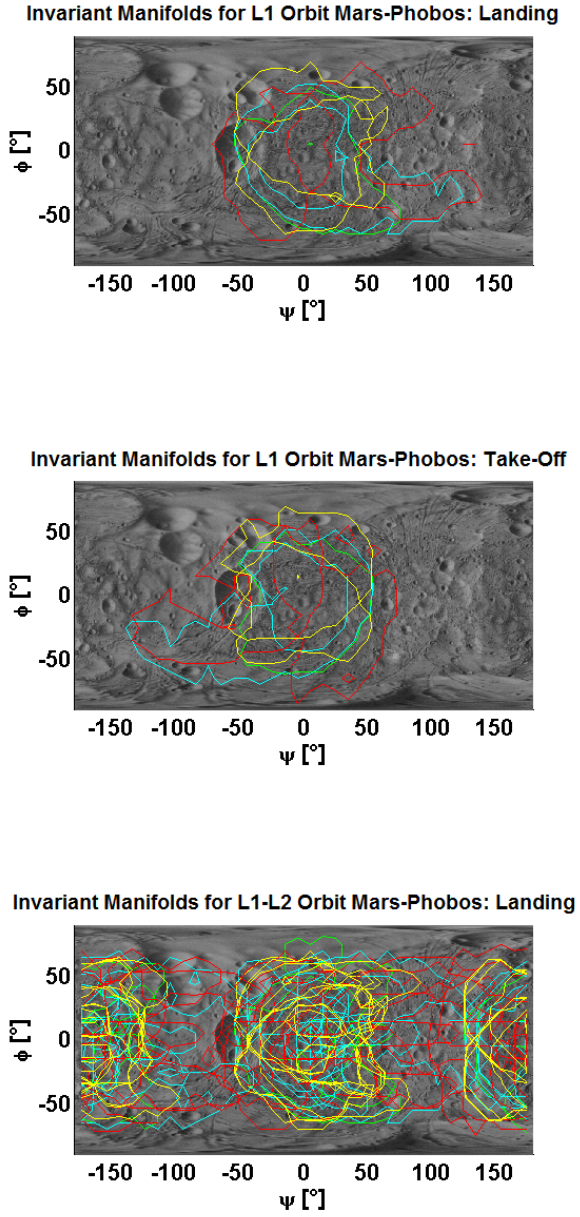

Figure 20: **IMs of the artificial LPOs with constant acceleration in the Mars-Phobos CR3BP-GH.** First two figures show the possible landing/take-off sites through the IM of the family A of POs around L_1, third figure shows the region of landing sites for all the families of artificial LPOs around L_{1-2}. Constant acceleration magnitude of $1mm/s^2$ along all coordinate axes directions (green line for CR3BP-GH, cyan for directions $\pm\hat{\mathbf{x}}$, red for directions $\pm\hat{\mathbf{y}}$, yellow for directions $\pm\hat{\mathbf{z}}$). Phobos shape harmonics.

trans-Phobos LPOs over the $70km$ altitude boundary of the Lyapunov stability region of the AEPs (the tip of the right leaf of Fig.11) become Floquet stable, while stable artificial LPOs along the y-axis are obtained displacing the equilateral LPs. Finally, displacing LPOs away from the natural SOI, in addition to reducing instability, it has other important advantages: indeed, all the problems of the dynamical modeling of the relative motion in proximity of this moon are related to the collapse of the realm of attraction of Phobos, therefore the manifold of LPOs is already too close in comparison to common interplanetary spacecraft operations (observations, science measures, descent start). Therefore, pushing inward Phobos with a simple constant propulsion profile enlarges the Phobos SOI, and there is a great advantage not only for mission operations constraints and light condition requirements, but in particular for the computational load of tracking these orbits: the effect of Phobos' gravity field quickly lowers with the distance, so the convergence of the solution of the LPOs (and so its reliability) will be obtained with a far lower order of the truncated GHs model to be used in the numerical continuation.

The IMs of the artificial periodic LPOs have been computed (Fig.20) and they have revealed that using constant thrust, along an appropriate direction, allows to enlarge the region of landing and take-off sites to cover all the longitude range (mostly with thrust along $\pm\hat{\mathbf{y}}$, but also inward Phobos), while the limit of the latitudes is also raised (thrust along $\pm\hat{\mathbf{z}}$) to become closer to the polar zones, that could be enclosed when considering also the families of QPOs. Also, the displacement of the LPOs away from Phobos and along the tangential axis enables artificial heteroclinic connections between two manifolds that were not possible with the natural dynamics: these trajectories could be exploited for fast orbital displacements around the two sides of Phobos for close-range mission segments.

6. Quasi-Satellite Orbits around Phobos

The last class of orbits that can be used in a mission to Phobos lies outside the SOI of the second massive body of a 3BP. The peculiar case of a small planetary satellite like Phobos is therefore very suitable for the exploitation of these orbits because of the collapse of its SOI, which indirectly drags the manifold of these orbits closer to the body. They

constitute a family of QPOs which are called by different names: Quasi-Satellite, Quasi-Synchronous, Distant Satellite, Distant Retrograde orbits. In particular, planar QSOs could be recognized as the quasi-periodic solution around the Strömgren's f class of periodic orbits of Hill's approximation of the planar CR3BP, as indicated in the seminal papers of Hénon [33, 34]. QSOs are more generally considered as one of three kinds of co-orbital configurations in a CR3BP with 1:1 resonance together with Tadpole and Horseshoe orbits: in [35] it is shown that unstable QSOs evolve from and to Horseshoe orbits, which are linked together. Another useful perspective is to relate the dynamics of QSOs to the relative motion between two close synchronous keplerian orbits around the primary body of the 3BP. This is the approach used in Formation Flying dynamics, where the osculating orbit of the secondary body, in our case Phobos, could be considered as a chief spacecraft orbiting Mars, that the third body follows in proximity. The solution of the keplerian synchronous Formation Flying in the Hill's rotating frame of the chief is a relative retrograde elliptical orbit, called epicycle [25]. This results in an artificial satellite of the secondary body, but due only to the attraction of the primary. Such an ellipse is defined in the rotating Hill's frame. The third body never rotates around the chief in the inertial frame, centered on the chief, where the third body remains at one side. Only thanks to the spinning rotation of the secondary body, that for the case of Phobos is synchronous with the Hill's frame rotation, the third body rotates in the BCBF frame of the secondary in 1:1 resonance. In particular, for slightly eccentric keplerian orbits (as in the case of Phobos) the epicycle resulting from a difference in eccentricity between third and secondary body is an ellipse centered on the chief, with major axis along the tangential Hill's axis and in 2:1 ratio with the minor axis; a difference in inclination or right ascension of ascent node inclines the epicycle, and the relative motion is 3D. The QSO is the motion of the epicycle when the chief is not a spacecraft but a second massive body, thus the QSO is the solution of the 3B dynamics. Therefore a QSO in the 3B problem is a QPO characterized by an oscillation of the whole epicycle along the y-axis of the 3BP frame. In addition, 3D epicycles experience a secular precession of their relative line-of-nodes: the related period grows as far as the size of the epicycle increases, which is the relative line-of-nodes becomes fixed in the Hill's frame (1:1 resonance).

The analysis of the QSOs around Phobos in this paper is conducted with the latter approach of a long-range Martian Formation Flying, in a keplerian perturbed (2B-P) model where the equations of motion are the Gauss' Planetary Equations [36], that use as state variable the equinoctial orbital elements (OEs) of the spacecraft around Mars, and the ER3BP is retained using as forcing action the 3B perturbation gravity of Phobos in the osculating Hill's frame centered on the moon. In terms of keplerian OEs, the QSO has short-period (rotation around Phobos along the epicycle) and medium-period (tangential motion of the epicycle) oscillations for semi-major axis, eccentricity and argument of pericenter, while the inclination and right ascension experience a long-period oscillation (precession of the epicycle): a 3D QSOs in the ER3BP is a torus with three phases. The 2B-P is suitable to be implemented with additional orbital perturbations: from our perturbation analysis in Section 2.3, we recover that outside of the Phobos' SOI, the major effects are due to the eccentricity (already embedded in the equations of motion) and the Mars J_2 GH. In particular, as a difference from the 3BP, in the 2B-P the orbital perturbations not due to Phobos are no longer differential. The differential action on the relative motion appears by computing in feedforward the osculating motion of Phobos and the angular velocity of its Hill's frame, with a dedicated 2B-P under the effect of the perturbation. Recall that when defining an initial condition for the QSO using mean OEs for the epicycle and Phobos and starting with true anomalies in accordance with the 2B dynamics, it produces different QSOs. The same QSO is obtained with osculating OEs in accordance to the perturbation, but their analytical expression is only available for particular cases, like J_2 [37], but not for the 3B perturbation. As an example, starting with the spacecraft in perimars and inferior conjunction, and starting in Mars-Phobos quadrature and phase in accordance on the same epicycle, it produces very different QSOs with the latter having a far lower amplitude of the y-axis oscillation.

The dynamical analysis of the QSOs requires the derivation of the secular derivatives of the 3B perturbation in the 2B-P, in a similar way to the case of J_2. But the solution of the mean integral value of the 3B perturbation could not be undertaken analytically. This integral is solved numerically in [35], and used for the stability analysis of the QSOs. The outcomes are two. First, any 2D

QSO large enough that the oscillation amplitude of the epicycle does not make it fall towards the secondary body (minimum distance of the epicycle) is always stable. Second, for any 3D QSO the secular precession will rotate the epicycle with the relative line-of-nodes towards the Hill's x-axis (relative nodes in conjunction with the two central bodies): such attitude becomes unstable as far as the inclination of the QSO increases, therefore the QSO leaves the body neighborhood and become a Horseshoe orbit. This 3D stability condition of the QSOs requires the difference in inclination (in radians) to be smaller than the difference in eccentricity. A linear Floquet stability analysis of QSOs in the CR3BP has highlighted the high stability of them [38]. In [39], a different approach has been undertaken, which is a linearized stability analysis in the ER3BP around the epicycle, and results are applied to the Mars-Phobos case. The minimum distance condition from Phobos is $29.4km$ ($\Delta e = 0.00315$), above which the planar QSO is stable. The 3D stability condition that bounds the admissible difference in inclination to the difference in eccentricity below which the inclined QSO is stable is $\Delta i/\Delta e < 96\%$. In addition, the period of the linearized precession motion is analytically derived. Similar numerical outcomes were obtained for the stability analysis of QSOs around Jupiter moon Europa [40]. In particular, we found that the minimum distance corresponds to a peculiar condition presented by Hénon in [34] on the stability of the planar QPOs around the f family of Hill's approximation of the planar CR3BP. As far as the dimension of the QPOs increases, the stability is influenced by resonances with the families of multiple-revolution direct satellite orbits, where the last resonance 1:4 is encountered by an epicycle of minimum distance equal to $1.2\sqrt[3]{\mu}$ of the orbital semi-major axis: after that, the QPO remains bounded even at infinite distance (within the Hill's approximation). This value for the Mars-Phobos system leads to a distance of $28.7km$, which is so close to the value obtained above in the linearized ER3BP. In addition, [34] found a very different sensitivity of the stability of the QPO between the two velocity components, with the radial one being far less critical. This means that the accuracy required by the GNC subsystem for the insertion manoeuver to the QSO is less critical in Mars-Phobos and Phobos-spacecraft common quadrature configurations, where the epicycle has only radial velocity on the orbital plane and the amplitude of the tangential oscillation is the smallest using mean OEs.

The stability of this class of orbits, combined with the collapse of the SOI and the synchronous rotation, makes the QSOs attractive solutions to orbit Phobos. A QSO will constitute the main orbital mission segment around Phobos for the upcoming Phootprint mission [41], to observe the surface thoroughly and identify the landing site where obtaining a sample of the soil to return back to Earth; it will be used for a very long time (6-9 months), and required to remain stable during the solar conjunctions that would black out the communications to the Earth for approximately 1 month. In this paper we probe the nonlinear stability of the QSOs around Phobos. Regarding Phootprint, the stability has been tested scanning the state-space in relative position and velocity with a true-life simulator [38]. Instead we conduct the analysis in the framework of the 2B-P (whose results, due to the fact that we are out of the Phobos SOI, are suitable to be interfaced with a previous orbital segment around Mars), and we use the linear stability region of [39] (a trapezoid in the plane Δe-Δi as shown in Fig.21) as a first guess in order to limit the boundary of the state-space in terms of osculating OEs where conduct the nonlinear simulations. We used the STK software, considering the default ephemerides of Phobos, starting at 10 April 2013 08:35:30UTCG (perimars), and the additional perturbations of the Mars GHs up to 15th degree/order, the Phobos GHs up to 4th degree/order, the Sun and SRP perturbations. We further limit the region by setting a range of minimum altitudes of the epicycle from Phobos between 20 and $60km$, therefore already inside the linear boundaries; regarding 3D QSOs the reference vertical size of Phobos is realized with just $\Delta i = 0.001rad = 0.06°$. We simulate QSOs up to one year of propagation time: a QSO is considered stable when it does not drift away by the end of the simulation. This is very reliable and not too much restricting because the strong nonlinearity of the 3B dynamics provokes behaviors drastically different crossing the stability region boundaries (as proved with the AEPs). The resulting true-life stability region boundary is presented in Fig.21: the minimum distance requirement is significantly higher than the linear one, and in the same range of Δe the 3D stability boundary is smaller than the linear one; for higher eccentricity such boundary asymptotically reaches the linear one. This stability region is related to positive Δe-Δi, while all the other initial conditions differences in osculating OEs at the

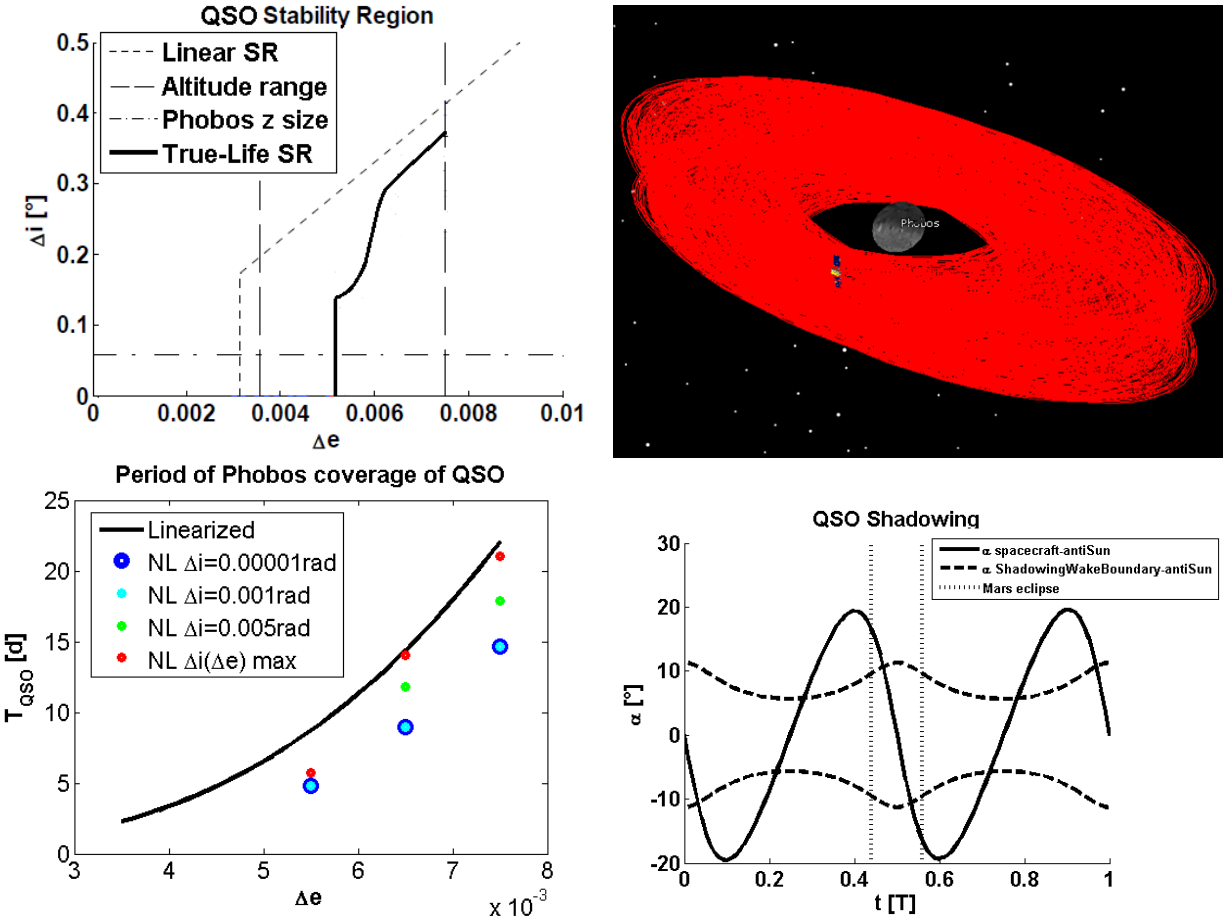

Figure 21: **QSOs around Phobos.** On the top-left, stability region of QSOs around Phobos tested by high-fidelity 1 year simulations, defined by initial conditions on osculating OEs around Mars for the spacecraft and Phobos: positive differences in eccentricity and inclination, starting at perimars epoch. On the top-right, example of a 3D stable QSO in the Phobos Hill's frame for 1 year propagation. On the bottom-left, period of precession of the relative line-of-nodes that indicates the minimum time for a complete Phobos surface coverage of the QSOs. On the bottom-right, example of the lighting conditions for a single keplerian epicycle at 50-110km distance range, remaining in the Mars and Phobos shadowing wakes for 34% of the time.

perimars are null. The starting Δe of the epicycle does not define trivially the minimum distance from Phobos of the QSO for the smallest range of eccentricities: the planar QSO at minimum stable Δe has a minimum altitude of 25km.

From a sample of trajectories simulated, the period of the secular precession for 3D QSOs was computed: this natural motion of the 3B dynamics is useful for observation purposes because it allows to overcome the 1:1 resonance of the keplerian epicycle and provide a complete coverage of the surface of Phobos. Fig.21 presents the related time required for the QSOs of the stability region, and compares it with the linearized solution from [39]: all the range of stable QSOs of interest provide a fast coverage of the moon. Another important performance that could be used in the mission design to select the optimal QSO inside the stable domain is the Δv of the insertion manoeuver: considering a previous mission segment realized by a Martian Trailing orbit (an AEP) with $\Delta\nu = [0°, -6°]$ from Phobos (corresponding to a distance 0-1000km), we computed the Δv budget to provide with the cheapest strategy of impulsive manoeuvers the initial conditions of the QSO Δe, Δi and the phasing $\Delta\nu$. Since Δe and Δi are small their cost range is moderate (5-7.5m/s and 0-8m/s), and also the cost of the phasing (0-20m/s) could be lowered for distant AEPs linearly performing multiple laps. The price to pay is instead the accuracy of the GNC subsys-

tem to insert precisely the spacecraft in this small range of initial conditions.

In this analysis we found a region of QSOs naturally stable with a high-fidelity perturbed model, potentially for a whole long-period mission scenario, with their distances from Phobos suitable for observation, and the exploitation of the natural precession motion provides a fast complete coverage of the surface of the moon. Such fast precession, combined with the exploitation of these orbits for long periods, allows a spacecraft to remain mostly in light. On the contrary, QSOs can be controlled to maintain a 1:1 resonance with Phobos BCBF frame: this would provide constant lighting conditions, ranging from continuous light (during solstices) to continuous shadow (during equinoxes), controlling the β-angle thermal condition desired by fine tuning the initial phase of the spacecraft along the epicycle with respect to the VDCO of the Sun around Phobos. An example in Fig.21 shows that a planar epicycle in the middle of the stability region, during an equinoctial season could remain in shadow from the field of view of the Sun for the 34% of the time.

7. Analysis of the Trade-offs and Applications in the Space Mission Design around Phobos

The trailing/leading orbits around Mars analyzed in Section 3, starting from $25km$ distance from Phobos, are attractive configurations, because they are cheap and affordable by SEP even for heavy human modules, they are stable to perturbations, and they are mostly in full light. They are the best orbits to start to approach Phobos SOI, however their ground-track on the moon is stationary and limited. Other distant configurations or close-range AEPs requires either high thrust or high station-keeping cost for hovering over long-time: they can be used only for short and dedicated operations of small unmanned spacecraft.

Keplerian orbits around Phobos are infeasible due to the collapse of the realm of attraction of the moon towards its surface. In Section 4 we investigated the artificial orbits around Phobos that would provide a spacecraft continuous light or shadow conditions moving synchronous with the Sun on its seasonal surface of motion. Due to the pull of Mars these VDCOs require continuous propulsion and they are too expensive even for few revolutions and also unstable.

Section 5 focuses on a class of interesting orbits that exist about Phobos, which are the LPOs. They are computed in an improved system of the relative dynamics in proximity of Phobos, upgrading the Mars-Phobos ER3BP system with the real gravity field of the moon, modeled with a gravity harmonics series expansion. These orbits are very close to the moon surface, therefore they are similar to close-range points but with an extended ground-track and range of lighting conditions, and the Phobos' bulk occultation of the sky could provide relevant passive shielding from the cosmic rays radiation. Despite their instability, the LPOs are natural motion and so will require no propulsion and low station-keeping cost to provide observation on Phobos and communication bridges to manage robotic scouts on Mars and Phobos: however, they require the high accuracy of an optical navigation subsystem, and high-load on the guidance subsystem, whose reference signal must be computed with advanced nonlinear techniques that need the acquisition of a high-fidelity gravity field of the moon. In particular, large quasi-periodic orbits enable coverage also of the polar and lead/trail-regions, and we found that in the Mars-Phobos elliptic system there exist tall and inclined periodic orbits around each side of the moon: a constellation, starting just from one spacecraft on each side, would fly synchronous and so enable stationary communications between most of the opposite sides of the moon (cis/trans, North/South, part of lead/trail) where different human crews or rovers could be displaced, as well as repeated access times to equatorial and middle latitude sites on Mars. Another useful application is to exploit their IMs as landing/taking-off gateways to and from the moon: in Section 5 we proved that there exist natural trajectories for a specific range of longitude-latitude sites able to land tangentially, facilitating a soft controlled touch-down, and depart with a very little escape velocity, less than 30% of the 2B Δv value. The optimization of these performances to select the best trajectory at a given location on Phobos will be paramount for sample-and-return missions (where also soil contamination avoidance is necessary) as well as first manned explorations of this moon. The addition of a simple propulsive law, to obtain a constant acceleration, offers some advantages when using these LPOs for short-phases. Section 5.1 shows that the surface coverage and landing/take-off targeting could be extended to the whole surface of Phobos, the instability of the orbits could be lowered, and the

Table 2: **Summary of orbits around Phobos.** First driver within a row is the altitude range (-). For IMs, (/) distinguishes the branch direction. Propulsive thrust range is indicated considering a 100/10,000kg spacecraft mass.

Orbit	Altitude Range	Reference Signal Computation	Dynamical Model	Orbital Propulsion	Maintainance Strategy			Surface Coverage	Lighting Conditions	Potential Mission Applications
					Control action	Guidance error	Navigation accuracy			
AEP	0-4.5km *x* 0m/s	relative fixed position, accurate gravity field model	C3B-GH	0.5/50-60N (150-180m/s²T) constant acceleration	unstable: SK 3.2m/s/T every 7-7min	10-10m 0.05-0.05m/s	1-1m 0.001-0.001m/s	stationary ground-track cis/trans-Phobos region	solstices: 50-80%; equinoxes: 40-70% (cis), 50-80% (trans)	dedicated proximity operations, radiation shield (35-37%)
	0-4.5km *y* 0m/s	relative fixed position, accurate gravity field model	C3B-GH	0.5/50-0.3/30N (150-100m/s²T) constant acceleration	unstable: SK 0.6-0.6m/s/T every 14-15min	10-10m 0.02-0.02m/s	1-1m 0.001-0.001m/s	stationary ground-track lead/trail Phobos region	solstices: 50-80% equinoxes 45-75%	dedicated proximity operations, radiation shield (36-16%)
	0-4.3km *z* 0m/s	relative fixed position, accurate gravity field model	C3B-GH	1/100-0.4/40N (300-120m/s²T) constant acceleration	unstable: SK 0.9-0.9m/s/T every 11-12min	10-10m 0.03-0.02m/s	1-1m 0.001-0.001m/s	stationary ground-track North/South pole Phobos region	S/W solstice: North/South light, South/North shadow; under 14km than light, equinoxes: 88%	dedicated proximity ops, complete lighting/shadowing, radiation shield (38-20%)
	4.5-70km *x* 0m/s	relative fixed position	C3B	0.6/0-1.5/150N (6-400m/s²T) constant acceleration	unstable: SK 6-20m/s/T every 13-9min	100-100m 0.2-0.3m/s	10-10m 0.01-0.01m/s	stationary ground-track cis/trans-Phobos region	solstices: light equinoxes: 88%	short close observation
	4.5-60km *y* 0m/s	relative fixed position	C3B	0.3/30-0.04/4N (100-12m/s²T) constant acceleration	unstable: SK 3-3m/s/T every 20-21min	100-100m 0.2-0.2m/s	10-10m 0.01-0.01m/s	stationary ground-track lead/trail Phobos region	solstices: light equinoxes: 88%	long close observation
	4.5-250km *z* 0m/s	relative fixed position	C3B	0.4/40-1.5/150N (120-400m/s²T) constant acceleration	unstable: SK 3-20m/s/T every 20-9min	100-100m 0.2-0.5m/s	10-10m 0.01-0.01m/s	stationary ground-track North/South pole Phobos region	solstices: light equinoxes: 88%	short close observation
	70-4600km *x* 0m/s	relative periodic orbit - cis/trans-Mars orbit	E3B - 2B(Mars)	1.5/150-6/600N (420-2000m/s²T) feedforward profile	stable	1-10km 0.5-2m/s	0.1-1km 0.01-1m/s	stationary ground-track cis/trans-Phobos region	solstices: light equinoxes: 88%	short stand-by, measurements, observation, comm-relay
	60-500km *v* 0m/s	relative periodic orbit - lead/trail-Mars orbit	C3B - 2B(Mars)	0.04/4-0.000440.04N (12-0.12m/s²T) feedforward profile	stable	0.1-10km 0.05-2m/s	0.01-1km 0.01-0.1m/s	stationary ground-track lead/trail-Phobos region	solstices: light equinoxes: 88%	long stand-by, measurements (acquisition of Phobos orbit and GM), comm-relay
	250-1400km *z* 0m/s	North/South-Mars orbit	2B(Mars)	1.5/150-8/800N (420-2500m/s²T) feedforward profile	stable	10-50km 2-10m/s	1-10km 0.1-1m/s	stationary ground-track North/South pole Phobos region	solstices: light equinoxes: 88%	short stand-by, measurements, observation, comm-relay
VDCO	0-10km 2-7m/s	relative circular equatorial orbit daily Sun-synch	2B(Phobos)	0.5/80-0.3/30N (100-50m/s²T) feedforward profile	unstable: SK 30-45m/s/T every 7-15min	100-100m 0.5-0.2m/s	10-10m 0.01-0.01m/s	equatorial swath	fixed, controllable (solstices: 0-100%, equinoxes: 0-88%)	fixed light/shadow conditions (directional solar radiation protection), comm-relay
	10-100km 7-30m/s	relative circular orbit at height 0-0/10-50km daily Sun-synch	2B(Phobos)	0.3/30-1.5/150N (50-250m/s²T) feedforward profile	unstable: SK 6-30m/s/T every 38-21min	1-1km 1-1.5m/s	100-100m 0.1-0.1m/s	hemispheric sector	fixed, controllable (solstices: 0-100%, equinoxes: 0-88%)	fixed light/shadow conditions (directional solar rad protection), hemisphere comm-relay
$L_{1,2}$-LPO	0-10km 0-8m/s	relative periodic (2:1) or quasi-periodic orbit, high-computational techniques, accurate gravity field model	E3B-GH	not required	unstable: SK 0.15-0.05m/s/T every 20-32min	10-10m 0.02-0.01m/s	1-1m 0.001-0.001m/s	stationary ground-track on wide Phobos region	solstices: 100-60% equinoxes: 86-50% (cis), 88-60% (trans)	short close observation, approaching manoeuvres comm-bridges, radiation shield (23-13%)
	0-80km 0-20m/s	relative periodic (8:M) or quasi-periodic orbit, high-computational techniques, accurate lighter gravity field model	E3B-GH - E3B	0.0/0-1.5/150N (0-400m/s²T) constant acceleration	unstable: SK 0.15-0.2m/s/T every 19-98min	10-100m 0.02-0.05m/s	1-10m 0.001-0.01m/s	stationary ground-track on dedicated region of whole Phobos surface	solstices: 100-60% equinoxes 88-59%	short dedicated ops, radiation shield (35-37%) - short standby, measurements (Phobos gravity field), comm-relay
1M-LPO	0-10km / 0-500km 0-15m/s / 0-60m/s	relative trajectory from LPO / Mars orbit 0.5-2h / 10-20h	E3B-GH	not required	SK 0.02m/s every 20min / 3m/s every 70min	10m / 1km 0.02m/s / 0.5m/s	1m / 100m 0.001m/s / 0.1m/s	landing site cis/trans-Phobos region / stationary ground-track lead/trail-Phobos region	controllable by epoch 0-100% / solstices: light, equinoxes: 88%	natural performanced soft landing (from 0.5g) /approach to Phobos or insertion manoeuvear to LPO
	0-10km / 0-500km 0-15m/s / 0-60m/s	relative trajectory from take-off site / LPO 0.5-2h / 10-20h	E3B-GH	not required	SK 0.02m/s every 20 min / 3m/s every 70min	10m / 1km 0.02m/s / 0.5m/s	1m / 100m 0.001m/s / 0.1m/s	take-off site cis/trans-Phobos region / stationary ground-track lead/trail-Phobos region	controllable by epoch 0-100% / solstices: light, equinoxes: 88%	natural performanced cheap take-off (from 3m/s) to LPO / escape from Phobos
	0-20km / 0-500km 0-25m/s / 0-60m/s	relative trajectory from LPO / Mars orbit 0(..1)h / 8-20h	E3B-GH - E3B	0/0-0.1/10N (0-10m/s / 0-100m/s) constant acceleration	SK 0.02-0.05m/s every 20 min / 2-3m/s every 70min	10m / 1km 0.02m/s / 0.5m/s	1m / 100m 0.001m/s / 0.1m/s	landing site on dedicated region of whole Phobos surface (apart near poles) / stationary ground-track lead/trail-Phobos region	controllable by epoch 0-100% / solstices: light, equinoxes: 88%	performanced soft landing (from 0.5g) /approach to Phobos or insertion manoeuvear to LPO
	0-20km / 0-500km 0-25m/s / 0-60m/s	relative trajectory from take-off site / LPO 0(..1)h / 8-20h	E3B-GH - E3B	0/0-0.1/10N (0-10m/s / 0-100m/s) constant acceleration	SK 0.02-0.05m/s every 20min / 2-3m/s every 70min	10m / 1km 0.02m/s / 0.5m/s	1m / 100m 0.001m/s / 0.1m/s	take-off site on dedicated region of whole Phobos surface (apart near poles) / stationary ground-track lead/trail-Phobos region	controllable by epoch 0-100% / solstices: light, equinoxes: 88%	performanced cheap take-off (from 3m/s) to LPO / escape from Phobos
	20-500km / 20-500km 0-60m/s / 0-60m/s	relative trajectory from LPO, take-off site / Mars orbit, LPO, take-off site 3-13h / 5-15h	E3B-GH / E3B	0.1/10-1/100N (10-500m/s / 50-600m/s) constant acceleration	SK 0.1-0.5m/s every 20min / 1-2m/s every 70min	10m / 1km 0.02m/s / 0.5m/s	1m / 100m 0.001m/s / 0.1m/s	dedicated ground-track / stationary ground-track lead-trail-Phobos region	controllable by epoch 0-100% / solstices: light, equinoxes: 88%	transfer manoeuver around Phobos / approach/escape to/from Phobos or insertion manoeuver to LPO
QSO	25-200km 8-50m/s	relative quasi-periodic orbit, high-fidelity simulations	2B(Mars)-P	not required	naturally stable without SK	10-100m 0.01-0.1m/s	10-100m 0.01-0.1m/s	complete in 5-25days	solstices: light equinoxes: 88%	parking orbits (repairs, refuelling), mission- control, Phobos-proximity facility, remote fast mapping and frequent access comms
	40-100km 10-25m/s	relative quasi-periodic orbit, high-fidelity simulations	2B(Mars)-P	if required by β-angle control system	naturally stable without SK	10-100m 0.01-0.1m/s	10-100m 0.01-0.1m/s	stationary swath	adjustable by dedicated control system	long stand-by, comm-relay, control of lighting conditions (directional solar radiation protection)

computation of the orbits themselves could be simplified to maintain them periodic also in the true elliptic dynamics, and to lower the accuracy of the model of the gravity field of the moon to be taken into account. In particular, artificial heteroclinic connections would now exist for fast orbital fly-bys around two opposite sides of Phobos.

Finally, the QSOs are discussed in Section 6, and they are the best solution for a precursor unmanned mission to Phobos. They are both natural orbits with no need of propulsion, and self-stable up to very long time with no need of station-keeping, and so they can be used as parking orbits with distance starting from $25km$ from Phobos. In particular, closer 3D QSOs provide a fast complete coverage to map the surface of Phobos and identify the landing site, and they are mostly in light. 2D QSOs during equinoctial seasons are suitable to be controlled to provide nearly Sun-synchronous orbits around Phobos, enabling constant and adjustable lighting conditions: in particular, lighting condition scheduling could be important for a first-generation manned spacecraft while orbiting Mars.

8. Conclusions

In this paper we analyzed several kinds of orbits around the Martian moon Phobos, each one defined using appropriate models of the relative dynamics where the reference signal is computed. The design of a future space mission to Phobos requires multiple objectives and constraints to be satisfied: we collect the outcomes of our analysis in Table 2, where each orbit has a number of potential applications and their performance can be assessed against the requirements of each mission segment.

A possible mission scenario for Phobos could be to start from establishing a trailing orbit around Mars, with a phasing of 0.4-1.2°, requiring a thrust to be maintained of less than 0.05-5N in accordance to the class of spacecraft, where start to track the real position of Phobos and acquire its gravity parameter. Then perform a phasing manoeuver to reach a QSO at an intermediate distance from Phobos, where start to measure the real gravity field and map the surface of the moon. Finally, move along the tube of the artificial invariant manifolds displaced away from the moon with a constant acceleration along the x-axis, whose LPOs tracking is less affected in their numerical computation by the GHs perturbations, to directly reach with a probe the desired landing site on Phobos. In the case of a sample-and-return mission, we then move in reverse choosing the trajectory that provides the minimum escape velocity, reaching a mothership that has been left on a closer LPO or parked in the QSO, to remotely command the lighter probe. In particular, the long-time stability of the QSOs around Phobos could be exploited as an orbital repository to send, in advance, unmanned propulsion modules, fuel stockpiles, and provisions, to remain parked in a secure low altitude Martian orbit without orbital maintenance costs and with short-period phasing manoeuvers to dock the modules. To allow the first human expeditions to visit Mars and return to the Earth, the spacecraft could make scheduled pit-stops at this orbital garage on Phobos' orbit.

Acknowledgments

This work has been supported by the European Commission through the Marie Curie fellowship PITN-GA-2011-289240 "AstroNet-II". We are thankful with Prof. J.J. Masdemont and Prof. G. Gómez (IEEC) for the assistance provided in the computation of LPOs in the CR3BP through high-order series expansions, and with Dr. J. Fontdecaba and Dr. V. Martinot (Thales Alenia Space) for providing the opportunity and the assistance of undertaking the applied research of the QSOs around Phobos.

References

[1] J. F. Bell, F. Fanale, D. P. Cruikshank, Chemical and physical properties of the Martian satellites, in: Resources of Near-Earth Space, Space Science Series, The University of Arizona Press, 1993, pp. 887–901.

[2] P. Rosenblatt, The origin of the Martian moons revisited, The Astronomy and Astrophysics Review 19 (44).

[3] E. K. Gardner, Evidence of life on Mars could come from Martian moon, `www.purdue.edu/newsroom/general/2012/120628T-MeloshHowellPhobos.html`, [Online] (28 June 2012).

[4] B. K. Sharma, Theoretical formulation of the Phobos, moon of Mars, rate of altitudinal loss, arXiv(0805.1454), [e-prints] (May 2008).

[5] ESA Media Relations Office, N°37-2012: European ministers decide to invest in space to boost Europes competitiveness and growth, `www.esa.int`, [Online].

[6] D. Koschny, Phootprint: An ESA mission study, in: Mars Concepts and Approaches Workshop, Houston, 2012 June 12-14.

[7] R. Staehle, L. Friedman, Interplanetary cubesats to the Moon and beyond, in: 1st International Workshop on LunarCubes, Palo Alto, 2012 November 13.

[8] J. B. Hopkins, W. D. Pratt, Comparison of Deimos and Phobos as destinations for human exploration,

and identification of preferred landing sites, in: AIAA Space 2011 Conference & Exposition, Long Beach, 2011 September 27-29.
[9] P. Lee, Phobos and Deimos update, in: 7th SBAG Meeting, Pasadena, 2012 July 10-11.
[10] A. Rivkin, NEO-Phobos-Deimos strategic knowledge gaps: Special action team final report, in: NASA SBAG Meeting, 2012 November 28.
[11] P. Abell, D. Beaty, D. Bass, J. Castillo-Rogez, T. Colaprete, S. Hoffman, R. Lewis, D. Mazanek, Instruments needed for a human exploration mission of Phobos and Deimos, in: International Workshop on Instrumentation for Planetary Missions, NASA Goddard Space Flight Center, 2012 October.
[12] M. Pandika, Stanford researchers develop acrobatic space rovers to explore moons and asteroids, news.stanford.edu/news/2012/december/rover-mars-phobos-122812.html, [Online] (December 28 2012).
[13] M. S. Wallace, J. S. Parker, N. J. Strange, D. Grebow, Orbital operations for Phobos and Deimos exploration, in: AIAA-AAS Astrodynamics Specialist Conference, Minneapolis, 2012.
[14] B. F. Chao, D. P. Rubincam, The gravitational field of Phobos, Geophysical Research Letters 16 (8) (1989) 859–862.
[15] W. S. Koon, M. W. Lo, J. E. Marsden, S. D. Ross, Dynamical Systems, the Three-Body Problem and Space Mission Design, Springer-Verlag, New York City, 2011.
[16] T. C. Duxbury, J. D. Callahan, Pole and prime meridian expressions for Phobos and Deimos, The Astronomical Journal 86 (11) (1981) 1722–1727.
[17] A. R. Conrad, The 2009 report of the IAU working group on cartographic coordinates and rotational elements, Celestial Mechanics and Dynamical Astronomy, Special Report.
[18] P. J. S. Gil, QSO: Current state of the art and mission analysis results for a class of Phobos observation and access orbits, in: 3rd International Workshop on Spaceflight Dynamics and Control, Covilhã, 2007 October 9.
[19] S. McKenna-Lawlor, P. Gonçalves, A. Keating, G. Reitz, D. Matthiä, Overview of energetic particle hazards during prospective manned missions to Mars, Planetary and Space Science 63 (64) (2012) 123–132.
[20] Belgisch Instituut voor Ruimte-Aëronomie (BIRA-IASB), ESA/ESTEC TEC-SEE Section, SPENVIS: The space environment information system, www.spenvis.oma.be/intro.php, [Online].
[21] P. Gonçalves, A. Keating, P. Nieminen, MarsREM:the Mars Energetic Radiation Environment Models, in: 31st International Cosmic Ray Conference, Łódź, 2009 July 7-15.
[22] G. Reitz, Biological effects of space radiation, in: ESA Space Weather workshop, 1998.
[23] C. Pei, Solar energetic particle transport in the heliosphere, Ph.D. thesis, University of Arizona (2007).
[24] D. A. Vallado, Fundamentals of Astrodynamics and Applications, Kluwer Academic Publishers, Dordrecht, 2001.
[25] M. Zamaro, Coupled orbital and attitude SDRE control system for spacecraft formation flying, Master's thesis, Politecnico di Milano (2011).
[26] C. Bombardelli, J. Peláez, On the stability of artificial equilibrium points in the circular restricted three-body problem, Celestial Mechanics and Dynamical Astronomy 109 (2011) 13–26.
[27] C. Bombardelli, Stable artificial equilibrium points in the Mars-Phobos system, in: 1st IAA-AAS Conference on Dynamics and Control of Space Systems, Porto, 2012 March 19-21.
[28] R. J. McKay, M. Macdonald, J. D. Biggs, C. McInnes, Survey of highly non-keplerian orbits with low-thrust propulsion, Journal of Guidance, Control and Dynamics 34 (3) (2011) 645–666.
[29] G. Gómez, J. J. Masdemont, C. Simó, Lissajous orbits around Halo orbits, Advances in Astronautical Sciences 95 (1997) 117–34.
[30] G. Gómez, J. M. Mondelo, The dynamics around the collinear equilibrium points of the RTBP, Physica D 157 (4) (2001) 283–321.
[31] M. Zamaro, J. D. Biggs, Dynamical systems techniques for designing libration point orbits in proximity of highly-inhomogeneous planetary satellites: Application to the Mars-Phobos elliptic three-body problem with additional gravity harmonics, in: 2014 International Congress on Nonlinear Problems in Aviation and Aeronautics: 10th International Conference on Mathematical Problems in Engineering, Aerospace, and Sciences, Narvik, 2014 July 15-18.
[32] M. Zamaro, J. D. Biggs, Natural motion around the Martian moon Phobos: The dynamical substitutes of the libration point orbits in an elliptic three-body problem with gravity harmonics, Celestial Mechanics and Dynamical Astronomy 122 (3) (2015) 263–302.
[33] M. Hénon, Numerical exploration of the restricted problem V. Hill's case: Periodic orbits and their stability, Astronomy and Astrophysics 1 (1969) 223–238.
[34] M. Hénon, Numerical exploration of the restricted problem VI. Hill's case: Non-periodic orbits, Astronomy and Astrophysics 9 (1970) 24–36.
[35] S. Mikkola, K. Innanen, P. Wiegert, M. Connors, R. Brasser, Stability limits for the Quasi-Satellite orbit, Monthly Notices of the Royal Astronomical Society 369 (2006) 15–24.
[36] R. H. Battin, An Introduction to the Mathematics and Methods of Astrodynamics, American Institute of Aeronautics and Astronautics Inc., Renston, 1999.
[37] Y. Kozai, The motion of a close Earth satellite, Astronomical Journal 64 (1959) 367.
[38] P. J. S. Gil, J. Schwartz, Simulations of Quasi-Satellite orbits around Phobos, Journal of Guidance, Control and Dynamics 33 (3) (2010) 901–914.
[39] F. da Silva Pais Cabral, On the stability of Quasi-Satellite orbits in the elliptic restricted three-body problem, Master's thesis, Universidade Técnica de Lisboa (2011).
[40] T. Lam, G. J. Whiffen, Exploration of Distant Retrograde orbits around Europa, in: 15th AAS-AIAA Space Flight Mechanics Conference, Copper Mountain, 2005 January 23-27.
[41] ESA/ESTEC, Mission analysis guidelines for Martian moon sample return. Final report (2012).